공학석사학위논문

Fatigue Reliability Evaluation of In-service Steel Bridge Using Measured Strain and BWIM Data

변형률 및 BWIM 계측 데이터를 활용한 공용 중 강 교량의 피로 신뢰도 평가

2022 년 2 월

서울대학교 대학원

건설환경공학부

이 상 현

Fatigue Reliability Evaluation of In-service Steel Bridge Using Measured Strain and BWIM Data

변형률 및 BWIM 계측 데이터를 활용한 공용 중 강 교량의 피로 신뢰도 평가

지도교수 김 호 경

이 논문을 공학석사 학위논문으로 제출함
2022년 2월

서울대학교 대학원
건설환경공학부
이 상 현

이상현의 공학석사 학위논문을 인준함
2021년 12월

위 원 장 _____ (인)

부 위 원 장 _____ (인)

위 원 _____ (인)

ABSTRACT

Fatigue Reliability Evaluation of In-service Steel Bridge Using Measured Strain and BWIM Data

Sang Hyeon Lee

Department of Civil and Environmental Engineering

Seoul National University

Strain gauges and bridge weigh-in-motion (BWIM) are representative field measurements normally used for the fatigue evaluation of in-service steel bridges. To evaluate the reliability of fatigue damage accumulation, the effective stress range and number of stress cycles applied to fatigue-prone details should be estimated based on field-measured data of a target bridge. However, the procedure for using field measurements to estimate either the effective stress range or the number of stress cycles has not been explicitly presented. Furthermore, studies that have quantitatively compared the differences in fatigue evaluation results according to the field measurement type or BWIM data-processing techniques are still insufficient. In this study, the strain and BWIM data were measured simultaneously on an in-service steel bridge to evaluate the fatigue damage. Both a frame model and a shell-solid model were used to examine the accuracy of the structural analysis models when using BWIM data. Two approaches using BWIM data to

estimate effective stress and average daily stress cycles were investigated. In addition, parametric studies have been conducted on the effect of driving patterns on fatigue evaluation. The differences in the fatigue evaluation results based on the type of field measurement and driving patterns were quantitatively compared. As a result, the fatigue reliability evaluation could be sufficiently accurate even when only two dominant driving patterns were used for steel bridges with typical short-to-medium spans.

Keywords: Steel bridge, Fatigue, Reliability Evaluation, Field test, Strain, Bridge weigh-in-motion (BWIM), Finite element model

Student Number: 2020-22553

TABLE OF CONTENTS

LIST OF FIGURES

LIST OF TABLES

CHAPTER 1

INTRODUCTION

1.1 Research Background

Fatigue in steel is a process of initiation and growth of cracks under numerous repetitive loads. This process can occur at stress levels that are substantially lower than those associated with failure under static loading conditions. The most common civil engineering structures that must be examined for fatigue are bridges (Fisher et al., 1998).

As the service life of a bridge increases, fatigue damage continues to accumulate owing to the repetitive stress range generated on the bridge members when vehicles pass. Figure 1.1 shows examples of fatigue cracks in steel bridges reported in a precedent study (Fisher and Roy, 2011).

Figure 1.1 Fatigue cracks in steel bridge (Fisher and Roy, 2011)

Because the accumulation of fatigue damage can cause the failure of bridge members, a quantitative evaluation is necessary to ensure the safety of a bridge (Nyman and Moses, 1985; Chotickai and Bowman, 2006). AASHTO LRFD (AASHTO, 2020) classified welded and bolted details for steel bridges into categories A to E' according to the connected shape and stress direction of the bridge members. According to the category of fatigue-prone details of the target bridge, the fatigue life of the bridge can be evaluated based on the design S-N curve. The relationship between the nominal stress range and the number of stress cycles of the design S-N curve was determined from the experimental results obtained under constant-amplitude loading. Therefore, when evaluating the fatigue life of a bridge based on the design S-N curve, it is necessary to exclude the local stress concentration and convert the variable-amplitude stress range of the measured stress history into an equivalent constant-amplitude stress range.

1.2 Fatigue Evaluation Using Field-measured Data

Determining the repetitive stress range and the number of stress cycles is a vital task in fatigue evaluation. The repetitive stress range applied to bridge members can be evaluated using either the strain data of the fatigue-prone detail or the cumulative weights of the vehicles passing through the bridge measured via the bridge weigh-in-motion (BWIM). The number of stress

cycles was calculated from the stress spectrum, and the variable-amplitude stress range histogram can be converted into an equal number of constant-amplitude stress range histogram according to Miner's rule (Miner, 1945).

Fatigue evaluation using strain data is generally considered the most accurate approach (AASHTO, 2018). Various fatigue reliability evaluation methods have been proposed for applying the randomness of strain measurements as a probability distribution. Frangopol et al. (2008) proposed a method to evaluate the fatigue damage of in-service steel bridges by considering the uncertainty of field measurements. Kwon and Frangopol (2010) considered the variability in the effective stress range based on the cutoff change in the stress range. Deng et al. (2018) considered the daily variability in the effective stress range based on strain data gathered from long-term measurements. Mao et al. (2019) considered the monthly variability in the effective stress range and number of stress cycles from long-term measurements of strain data. In particular, if the data are insufficient owing to a short measurement period, it is necessary to consider the uncertainty by fitting the stress range spectrum to a continuous probability density function (Ni et al., 2010; 2012).

However, it is sometimes difficult to install strain gauges on fatigue-prone details, owing to rivets or welding. Installing strain gauges on all fatigue-prone details of bridges makes it unreasonable in terms of maintenance costs.

To solve these limitations, several studies have been conducted to probabilistically evaluate the fatigue damage of in-service steel bridges using BWIM data and structural analysis models of bridges instead of strain data. Fatigue reliability evaluations are performed by positioning vehicle loads based on a probabilistic model of axle loads and spacing as measured by BWIM along driving lanes (Guo et al., 2012), or on fatigue-prone details that demonstrate the worst load effects (Liu et al., 2016; Lu et al., 2017; Lu et al., 2019). In addition, fatigue reliability is evaluated using a time-series stress history that considers input from multiple presences from the lanes and vehicle speeds to calculate the stress spectrum (Yan, Luo, Lu, et al., 2017; Yan, Luo, Yuan, et al., 2017; Deng et al., 2021).

However, the driving patterns and accuracy of the structural analysis models were different for each study because the fatigue evaluation procedure for using BWIM data or structural analysis modelling was not specified in the evaluation manual. In addition, studies that have quantitatively compared the differences in fatigue evaluation results according to the type of field measurement, accuracy of the structural analysis model, and consideration of driving patterns are still insufficient.

1.3 Research Objective and Scope

This study presents a suggestion for using the available BWIM data from

a complete field experiment to produce a more reliable fatigue assessment of steel bridges with short-to-medium spans. The driving patterns considered in performing fatigue reliability evaluations can significantly affect the calculated fatigue life of the target bridge. Hence, field tests were performed to identify the influential parameters among the structural analysis options and the usage of field-measured data, and to determine the effect on the fatigue reliability assessment of the target bridge. To quantitatively compare the fatigue reliability evaluation results, field tests on an in-service steel bridge used simultaneous measurements of traffic loads and bridge responses based on the BWIM and strain gauges.

Chapter 2 describes the preparation process for evaluating the fatigue life of a target bridge. The basic information of the target bridge, category of fatigue-prone details, and field measurement are included. In addition, a frame model and a shell-solid model of the bridge were developed using commercial structural analysis programs. The effect of the accuracy of the structural analysis model on the evaluation of stress acting on the fatigue-prone detail by vehicle load was examined based on the validation results of the structural analysis model generated in two types.

Chapter 3 describes how to evaluate the fatigue life of a target bridge based on probabilistic techniques using field measurements. Two approaches for processing BWIM data were investigated. Approach 1 estimates the

equivalent truckload from the BWIM-measured gross vehicle weight (GVW) spectrum and positions the vehicle to the worst load effect in fatigue-prone details. Approach 2 generates an artificial time-series stress history by considering all BWIM-measured driving patterns, such as the entry time, driving lane, velocity, axle weights, and axle spacing of vehicles. The stress spectrum was calculated based on artificial stress history. According to each approach, fatigue reliability evaluations were performed by estimating the effective stress range (S_{eff}) and the average daily stress cycles (*ADSC*). The fatigue reliability index of each approach using BWIM data was quantitatively compared based on the fatigue reliability index evaluated using strain data.

In Chapter 4, three typical driving patterns that can be considered when performing fatigue reliability evaluation using BWIM data are investigated: headway, driving lane, and axle load distribution. Parametric studies were conducted to remove the relative influences of BWIM-measured driving patterns on fatigue reliability evaluation. The effect of each driving pattern on the fatigue life evaluation was confirmed by comparing the parametric study results with the fatigue reliability indices in Chapter 3. Consequently, parameters and evaluation procedures for reasonable fatigue life evaluation of bridges with typical short-to-medium spans were suggested.

Finally, Chapter 5 provides conclusions drawn based on the fatigue

reliability evaluation results. The importance and contributions of this study are also discussed.

CHAPTER 2

Field Tests and Analysis Models

2.1 Information of the Target Bridge

The Yong-du 1st Bridge, where the strain gauge and BWIM measurements were simultaneously performed, is a two-span steel composite bridge with a width of 25 m and length of 90 m (=2@45 m) located in Asan-si, Chungcheongnam-do, Republic of Korea. Figure 2.1 shows the target bridge.

Based on the AASHTO LRFD (AASHTO, 2020), the weld of the bottom flange and diaphragm located at the maximum moment section of box 1 of the target bridge was selected as a fatigue-prone detail. The fatigue category of the fatigue-prone detail was C'. A typical example of the base metal at the toe of a transverse stiffener-to-flange fillet weld is shown in Figure 2.2.

Figure 2.1 Yong-du 1st bridge

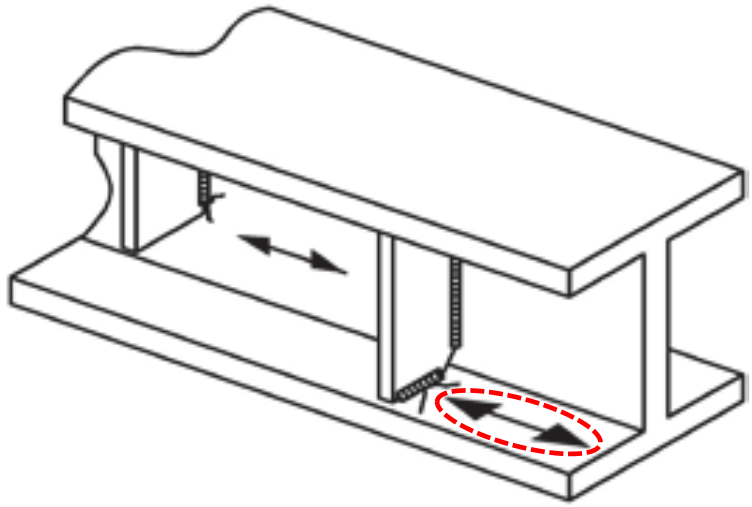

Figure 2.2 Welded stiffener-to-flange connection (AASHTO, 2020)

2.2 Field Measurement

Strain gauges were installed at one-quarter intervals on each span and 40% of the span length from both supports. The strain gauge installed on the fatigue-prone detail is 'SG-G1-4-B'. Figure 2.3 shows the installation locations of the strain gauges. The BWIM system was installed at a one-way two-lane entrance, as shown in Figure 2.4. Measurements were performed for a week from October 12th to 18th, 2019.

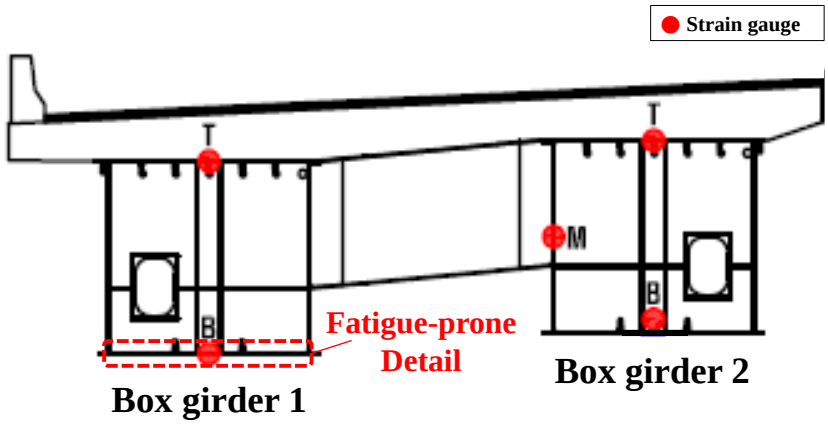

(a)

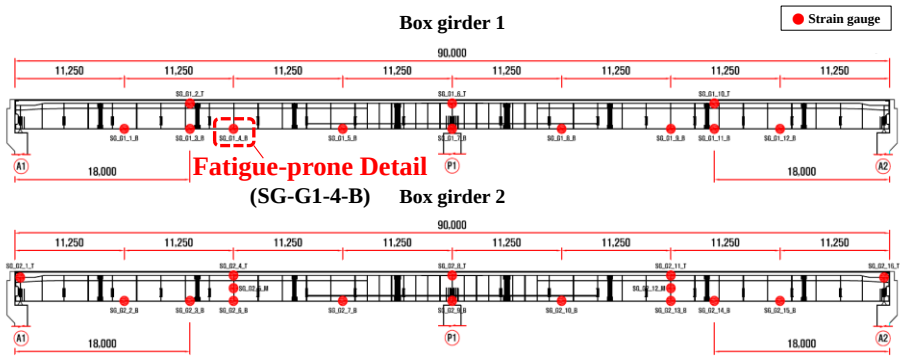

(b)

Figure 2.3 Location of the strain gauges and a fatigue-prone detail:

(a) cross-section, (b) side view

Figure 2.4 Installed BWIM system of the target bridge

2.3 Structural Analysis Model

The manual for bridge evaluation (MBE) (AASHTO, 2018) classifies structural analysis models as either simplified or refined to calculate the nominal stress acting on the fatigue-prone detail by vehicle loads. The most important difference between the two structural analysis models is whether the nominal stress applied to the fatigue-prone detail can be calculated directly. To examine the effect of the accuracy of the structural analysis model on fatigue reliability evaluation, two types of structural analysis models were developed for the target bridge using commercial structural analysis programs.

The information for each member and the material properties for the target bridge modelling are described in Appendix A.

2.3.1 Simplified Model

A three-dimensional frame model with a composite cross-section was developed using Midas civil (Midas IT, 2021). The simplified analysis model of the target bridge is shown in Figure 2.5(a), and the boundary conditions were set as shown in Figure 2.5(b) at the support node where each steel box met the pier. The frame model can be used to input the properties of the slab, web, flange, and longitudinal rib of the composite box girder section. However, there are limitations to inputting the diaphragm, horizontal stiffener, vertical stiffener, and details (i.e., fillet weld, rivet connection, and cutout).

The nominal stress applied to the fatigue-prone detail was calculated from the moment generated on the element by the vehicle load and distance from the neutral axis of the composite section to the bottom flange. Axle loads and spacing can be defined using the ‘moving load function’ in the program. In addition, the driving position of a vehicle was designated using the load-eccentricity function, and an influence line analysis of the nominal stress acting on the fatigue-prone detail was performed.

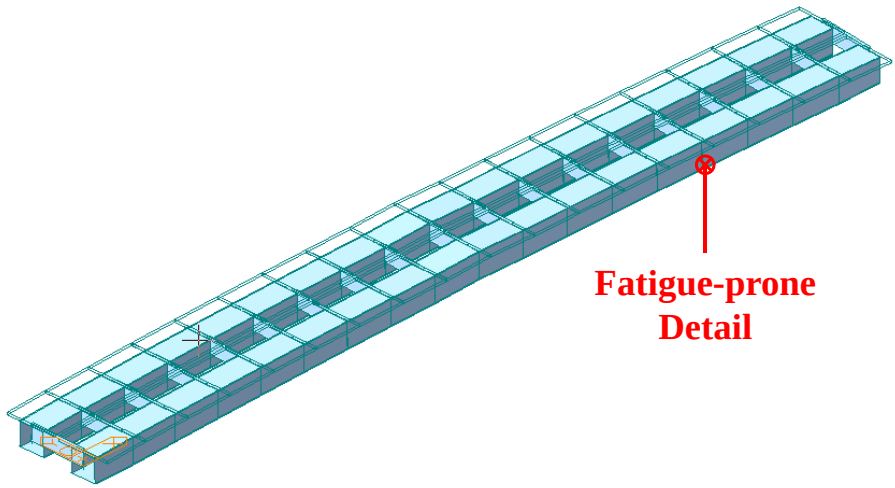

(a)

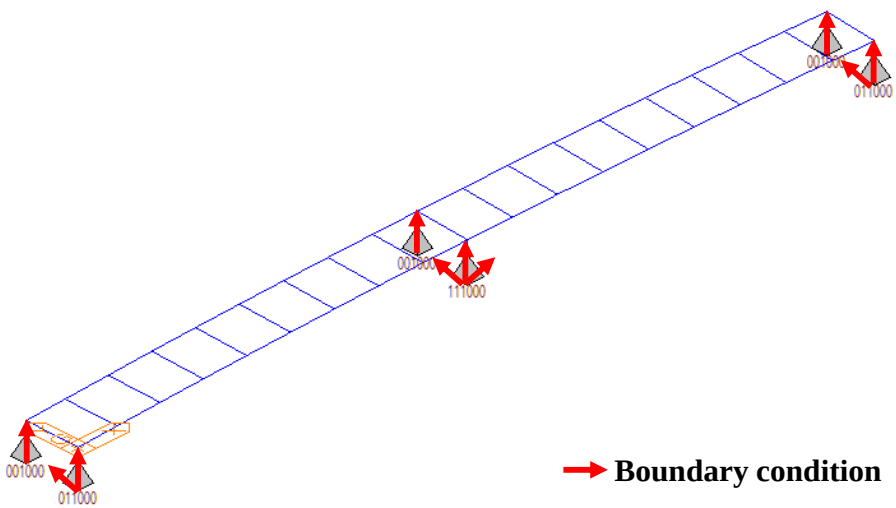

(b)

Figure 2.5 Frame model: (a) bridge model, (b) boundary conditions

2.3.2 Refined Model

A three-dimensional shell-solid model was generated using Abaqus (Dassault Systems, 2021). Two types of finite elements were used, as shown in Figure 2.6. Solid elements were used to model the bridge deck, and the steel box and crossbeam were modelled using shell elements. The solid element type is "C3D8 (8-node linear brick)," which is the most commonly used. For 'thin' shell elements with thickness less than 1/15 of the characteristic length, such as the distance between supports, the transverse shear flexibility can be neglected, and the Kirchhoff constraint must be satisfied accurately (i.e., the shell normal remains orthogonal to the shell reference surface). The shell element type is "S8R5 (8-node doubly curved thin shell, reduced integration, using 5-DOF per node)", which satisfies these conditions.

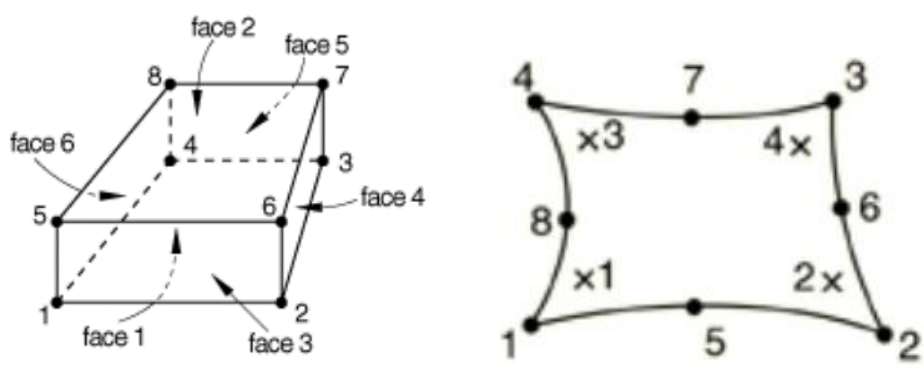

(a) **(b)**

Figure 2.6 Finite element: (a) Solid element, (b) Shell element

The refined analysis model of the target bridge is shown in Figure 2.7. Figure 2.8(a) shows the shoe placed on the support of the target bridge. To set boundary conditions similar to the real bridge, shoe elements of 500 mm × 500 mm were created and placed on the supports, as shown in Figure 2.8(b). For each DOF, the boundary conditions were set on the surface of the edges of the shoe support. The shell-solid model can implement most bridge elements and details. In this study, details related to the local stress concentration effect were not modelled because the nominal stress applied to the fatigue-prone detail is a major concern.

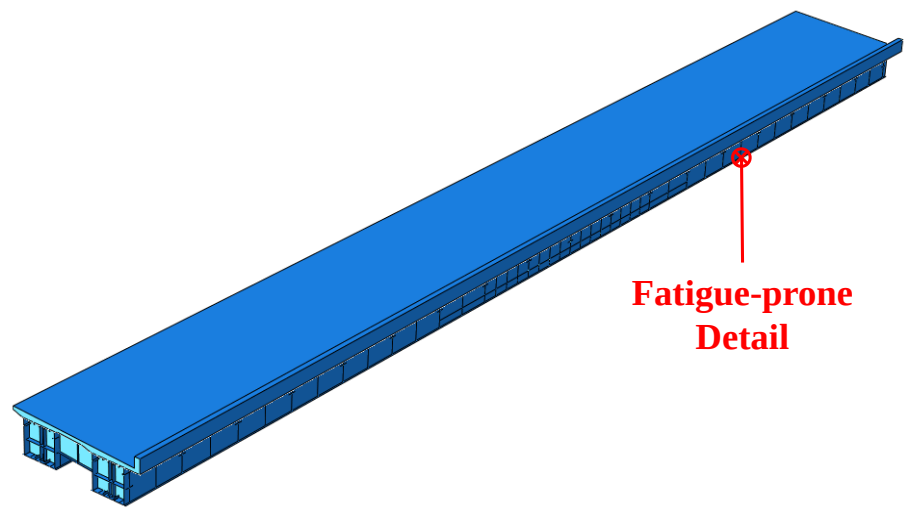

Figure 2.7 Shell-solid model

(a)

(b)

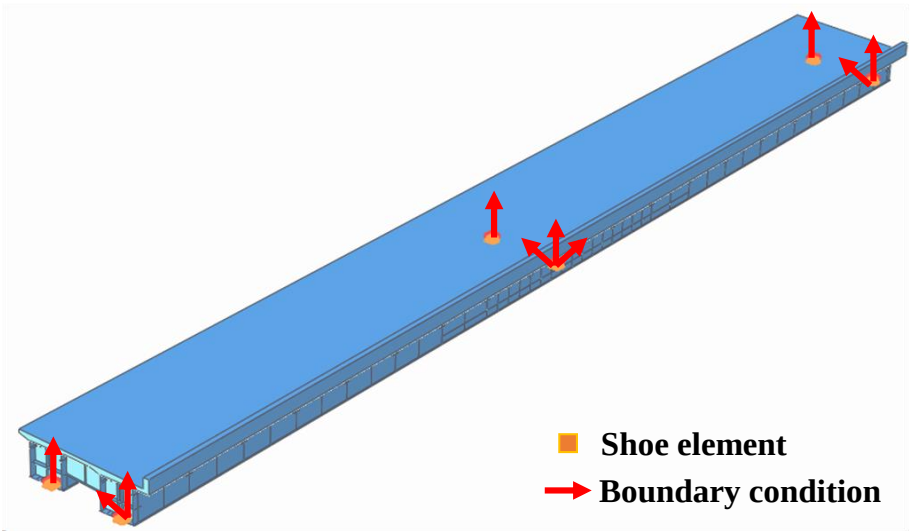

Figure 2.8 Support shoe: (a) target bridge, (b) modeling

The accuracy of the finite element analysis is affected by the mesh size of the element. Therefore, a convergence check for determining the mesh size must be preceded, which can be performed according to various criteria according to the purpose of the research. In this study, a self-weight analysis was performed to confirm the tensile stress of the maximum deflection part,

because the tensile stress occurring on the bottom flange is the most important indicator. In addition, since the two types of finite elements are combined, the convergence of the tensile stress according to the mesh size for each element was checked. The mesh size of the target element was changed to 50, 100, 150, 200, and 250 mm, while that of the other element was fixed at 200 mm. Figure 2.9 shows the convergence check results for each finite element type.

Consequently, it was confirmed that the mesh size of the solid elements constituting the concrete slab had little effect on the tensile stress of the bottom flange. In addition, the tensile stress according to the mesh size of the shell elements constituting the steel box girder was almost the same at 50 mm from 200 mm and decreased at 250 mm. Therefore, the mesh size of the shell and solid elements was determined to be 200 mm based on the convergence check results.

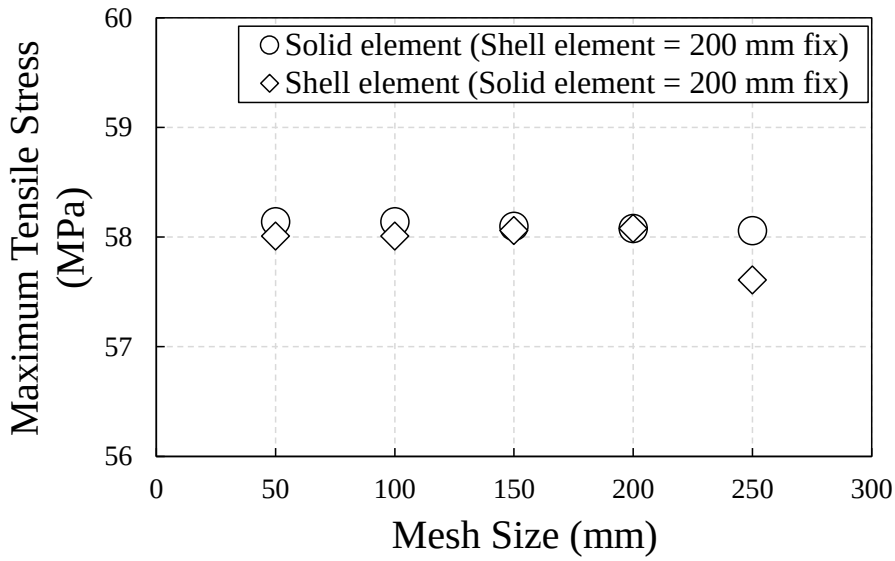

Figure 2.9 Convergence check results

To obtain the influence line of the nominal stress generated on the fatigue details, iterative static analyses were performed by moving a unit load. The unit load was applied using pressure to a rectangular wheel area of 200 mm × 600 mm, calculated based on Equation (2.1) of the Korean Highway Bridge Design Code (MOLIT, 2016).

$$A_W = \frac{12{,}500}{9} P \ (mm^2) \tag{2.1}$$

where, A_W is a rectangular wheel area, and P is a wheel load.

Because the nominal stress should be calculated as the membrane stress,

excluding the bending stress, the average of the upper and lower surfaces was taken. A precedent study shows that local stress concentration effects should be excluded to calculate the nominal stress of a finite element analysis model (Hobbacher, 2009). The nominal stress acting on the fatigue-prone detail was estimated by quadratic extrapolation, as shown in Figure 2.10. The reference points for extrapolation were located at 200, 400, and 600 mm along the longitudinal direction from the fatigue-prone detail.

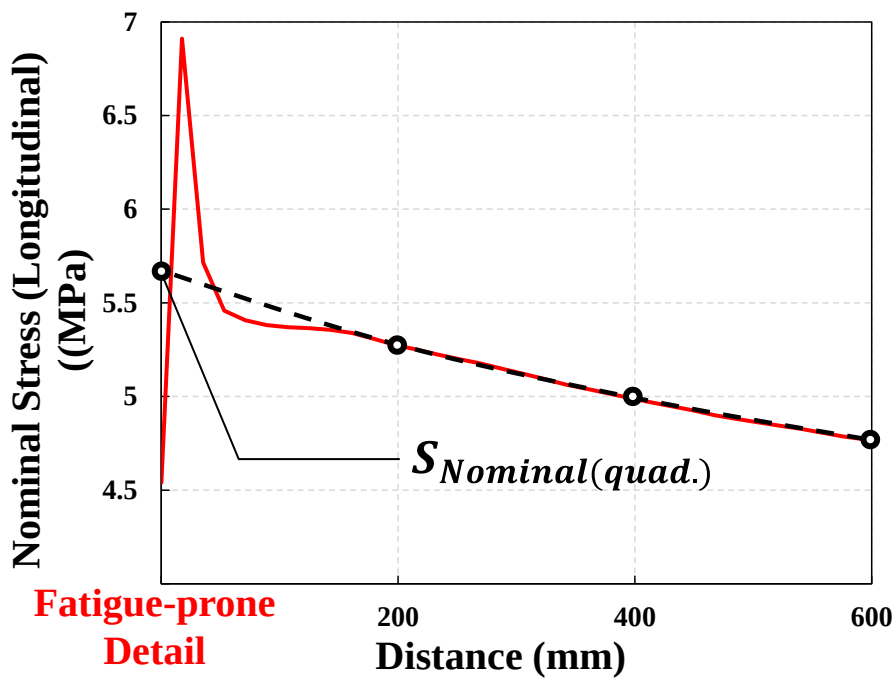

Figure 2.10 Quadratic extrapolation to determining nominal stress

2.4 Validation of Structural Analysis Model

To validate the two types of structural analysis models, cases in which a single vehicle was loaded onto the bridge were selected from the BWIM data. The measurements of the vehicle load from the BWIM data were applied to the two structural analysis models, and the difference between the calculated and measured stress ranges was obtained from the strain data.

Figure 2.11 compares the single vehicle cases. A total of 1,561 cases were identified as single vehicle loads during the entire measurement period, and the measured and calculated stress ranges are compared in Figure 2.12. Compared with the measured stress ranges from the strain data, the nominal stress ranges calculated using BWIM data averaged 12% and 4% larger in the frame model and shell-solid model, respectively. The difference between the analysis and measured results was the criterion for selecting the shell-solid model for further analysis.

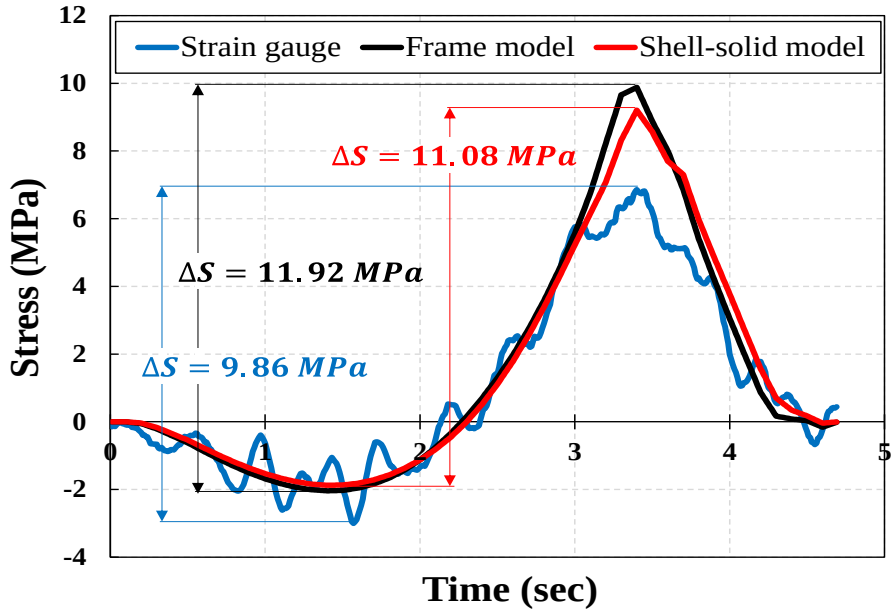

Figure 2.11 Measured and calculated stress time histories for a single vehicle loading

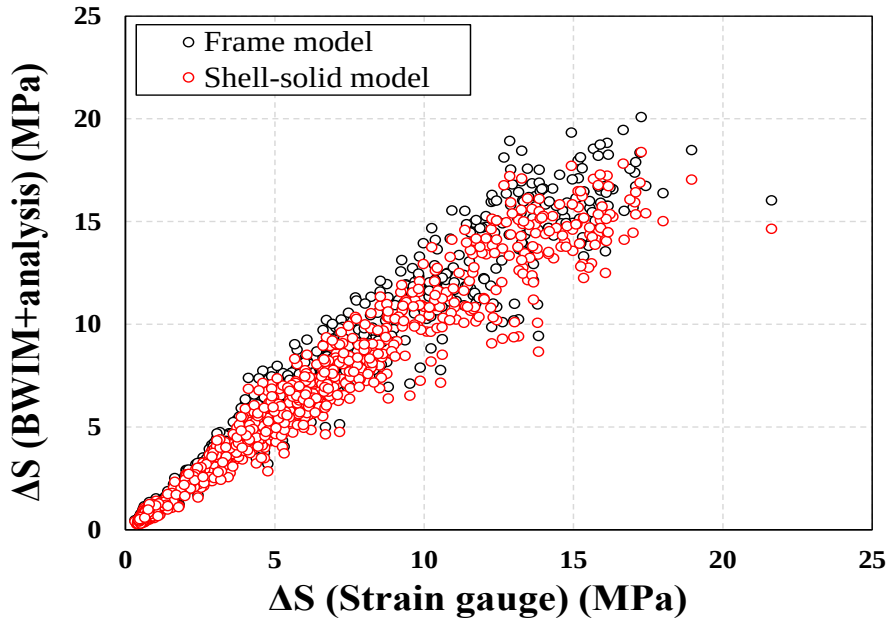

Figure 2.12 Calculated stress ranges according to two types of analysis model for all single vehicle cases

CHAPTER 3

Fatigue Reliability Evaluation

3.1 Fatigue Limit State

The limit state function of fatigue damage accumulation is defined by Equation (3.1) (Kwon and Frangopol, 2010). The fatigue damage accumulation is evaluated by the ratio of the stress cycles experienced during the service life and the limits of the stress cycles according to the fatigue category.

$$g(X) = \Delta - e \cdot D \tag{3.1}$$

where, Δ is the Miner's critical damage accumulation index in terms of resistance, e is the measurement error factor, and D is the accumulated fatigue damage defined in Equation (3.2).

$$D = \sum_i \frac{n_i(y)}{N_i} = \sum_i \frac{n_i(y) \cdot S_i}{A} \tag{3.2}$$

where, n_i is the number of cycles of the i[th] stress range (S_i) during the service life in the stress spectrum, and A is the detail-category coefficient.

The number of stress cycles applied to the fatigue-prone detail during the service life can be expressed as Equation (3.3) for the *ADSC* considering the annual traffic increase from the total stress cycles of the stress range histogram. In addition, the S_{eff} with the same number of stress cycles can be estimated as Equation (3.4) from the variable-amplitude stress range according to Miner's rule.

$$\sum_i n_i\,(\mathrm{y}) = 365 \cdot ADSC \cdot \int_0^y (1+\alpha)^y dy = 365 \cdot ADSC \cdot \frac{(1+\alpha)^y - 1}{ln(1+\alpha)} \tag{3.3}$$

where, α is the rate of annual traffic increase, and y is the number of years.

$$S_{eff} = \left[\sum_i \gamma_i\,(\Delta S_i)^3\right]^{\frac{1}{3}} \tag{3.4}$$

where γ_i is the fraction of cycles within the stress range ΔS_i.

From Equations (3.3) and (3.4), the cumulative fatigue damage in Equation (3.2) can be expressed as Equation (3.5) for the constant-amplitude S_{eff} and *ADSC*.

$$D = \sum_i \frac{n_i(y) \cdot S_i}{A} = 365 \cdot ADSC \cdot \frac{(1+\alpha)^y - 1}{ln(1+\alpha)} \cdot \frac{\left(S_{eff}\right)^m}{A} \qquad (3.5)$$

where, m is the material constant.

The parameters constituting the fatigue limit state function are described in Table 3.1.

Because most of the stress amplitudes that occur during the service life of a bridge are less than the constant-amplitude fatigue limit (CAFL), there is a risk of underestimating the fatigue damage of a bridge if the stress amplitudes at less than the CAFL are neglected. Therefore, several precedent studies have considered the stress ranges below the CAFL using a modified S-N curve based on experimental and analytical results (Kawada and Misawa, 1968; Connor et al., 2005; Yen et al., 2009; Kwon et al., 2012; Alencar et al., 2021). This study also adopted an extended S-N curve with a slope of 3 below the CAFL (Murakami et al., 2021), as shown in Figure 3.1.

The distributions of the random variables and constants for the parameters constituting the limit state function are listed in Table 1. The fatigue reliability

index (β) was estimated using the First-Order-Reliability-Method (FORM) to establish the service life.

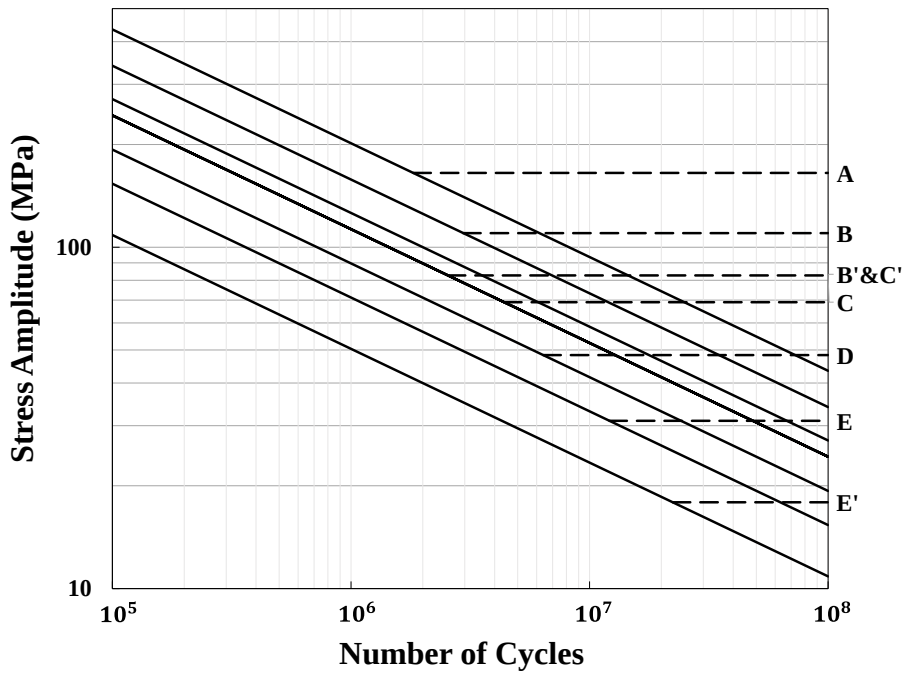

Figure 3.1 Extended S-N-curve (Murakami et al. 2021)

Table 3.1 Parameters for fatigue reliability evaluation

Parameter	Distribution		Reference
	Type	Value	
Miner's critical damage accumulation index, $\boldsymbol{\Delta}$	Lognormal	$\lambda_{\Delta} = 1, \zeta_{\Delta} = 0.3$	Wirsching, 1984
Measurement error, $\boldsymbol{e}$	Lognormal	$\lambda_{e} = 1, \zeta_{e} = 0.03$	Frangopol et al., 2008
Detail-category coefficient (MPa^3), $\boldsymbol{A}$	Lognormal	$\lambda_{A} = 23.11, \zeta_{A} = 0.15$	Keating and Fisher, 1986; Chung, 2004
Traffic increase rate (per year), $\boldsymbol{\alpha}$	Deterministic	0.0104	Shin et al., 2007
Material constant, $\boldsymbol{m}$	Deterministic	3	AASHTO, 2020
Time (year), $\boldsymbol{y}$	variable	increment = 0.1	

3.2 Estimation of S_{eff} and *ADSC* Using Strain Data

Among the measurements for one week, only data from the five days without measurement loss or error were used for the calculation. The stress range spectrum was extracted from the field-measured stress data via the rain-flow counting method (Downing and Socie, 1982), and the *ADSC* was calculated from the results. S_{eff} was estimated according to Miner's rule.

Stress ranges lower than 7 MPa, which had little effect on fatigue damage, were excluded by applying a cutoff level (Connor et al., 2004; Hodgson et al., 2006). Because the measured period was short, the stress range spectrum was fitted as a continuous probability density function using a Gaussian mixture model (GMM). The optimal number, weights, and parameters of the GMM components were obtained iteratively using the Akaike information criterion (AIC) (Akaike, 1974). In addition, the fitted result was certified by the one-sample KS test, and the null hypothesis was not rejected at the 5% significance level. Figure 3.2 shows the stress range spectrum measured in the fatigue-prone detail and the fitting result.

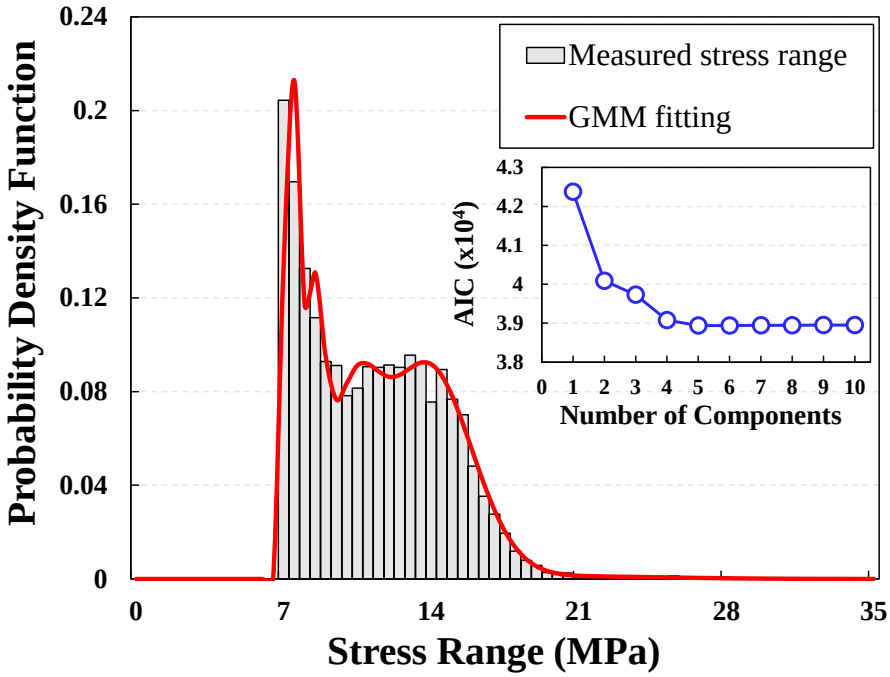

Figure 3.2 Measured stress range spectrum

3.3 Estimation of S_{eff} and *ADSC* Using BWIM Data

Prior to the estimation of S_{eff} and *ADSC*, some inaccurate measurement records of BWIM data were excluded in accordance with the precedent studies (Sivakumar et al., 2011; Kim and Song, 2019).

1) The difference between the measured GVW and the sum of the axle weights should be less than 10%.
2) GVW should be greater than 0.8 tons but less than 100 tons.
3) Vehicle length should be greater than 2 m but less than 36 m.
4) The smallest proportion of axle weight to GVW must be greater than

5%.

5) Headway should be longer than 0.3 seconds.

When fatigue evaluation is performed using BWIM data, S_{eff} and *ADSC* can be estimated via one of the two approaches. Approach 1 is a process for estimating the equivalent truckload (W_{eq}) and single-lane average daily truck traffic ($ADTT_{SL}$) from the GVW spectrum. The GVW spectrum was fitted as a continuous probability density function using GMM. Similarly, the optimal number, weights, and parameters of the GMM components were obtained iteratively using AIC, and the fitted results were certified by the KS test. Figure 3.3 shows the GVW spectrum and the fitting results.

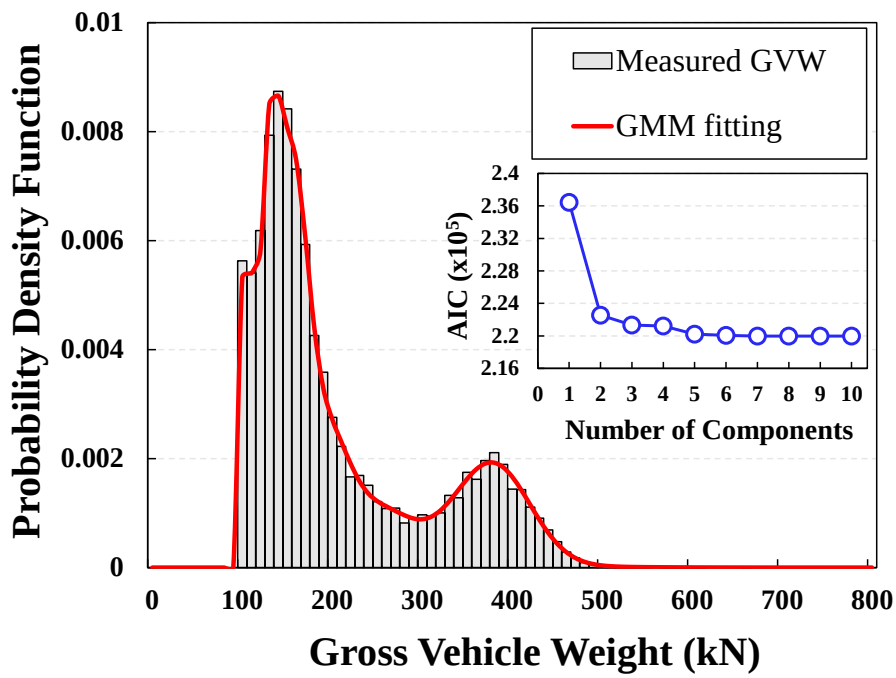

Figure 3.3 Measured GVW spectrum

W_{eq} was calculated using the root-mean-cube method shown in Equation (3.6) (Moses et al., 1987), and was applied to the location that causes the worst load effect on the fatigue-prone detail without considering traffic lanes. In this process, lightweight vehicles with contribution-to-fatigue damage of less than 100 kN were excluded from the calculation (Iatsko et al., 2020).

$$W_{eq} = \left[\sum_i f_i W_i^3\right]^{\frac{1}{3}} \tag{3.6}$$

where, f_i is the frequency of the GVW W_i.

S_{eff} can be estimated from the difference between the maximum and minimum nominal stress. To determine the vehicle location that caused the worst load effect, the influence surface of the nominal stress in the longitudinal direction was obtained, as shown in Figure 3.4(a). The influence line in Figure 3.4(b) shows the change in the nominal stress in the longitudinal direction according to the transverse position of the vehicle load at the location where the maximum nominal stress occurred. The nominal stress of the shell-solid model increased significantly as the vehicle load approached the location where the maximum stress occurred. The influence line for the longitudinal worst load effect can be extracted from the influence surface, as shown in Figure 3.4(c).

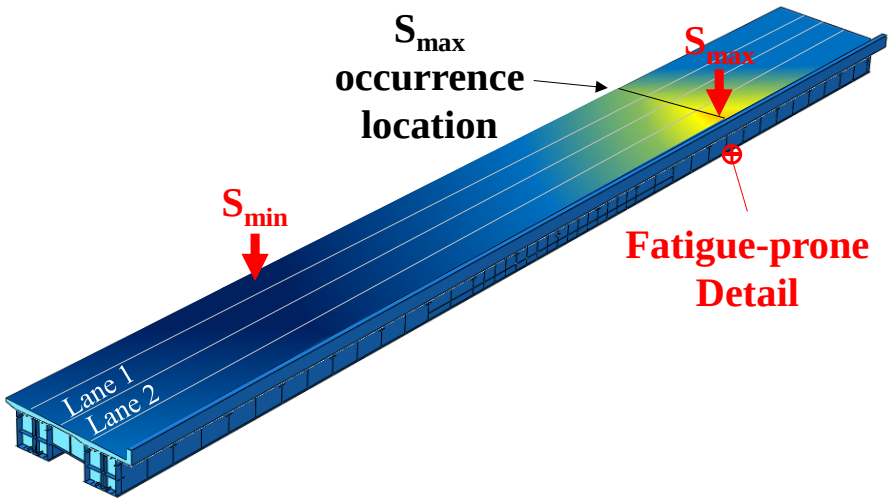
S_{max}
occurrence
location
S_{max}
S_{min}
Fatigue-prone
Detail
Lane 1
Lane 2

(a)

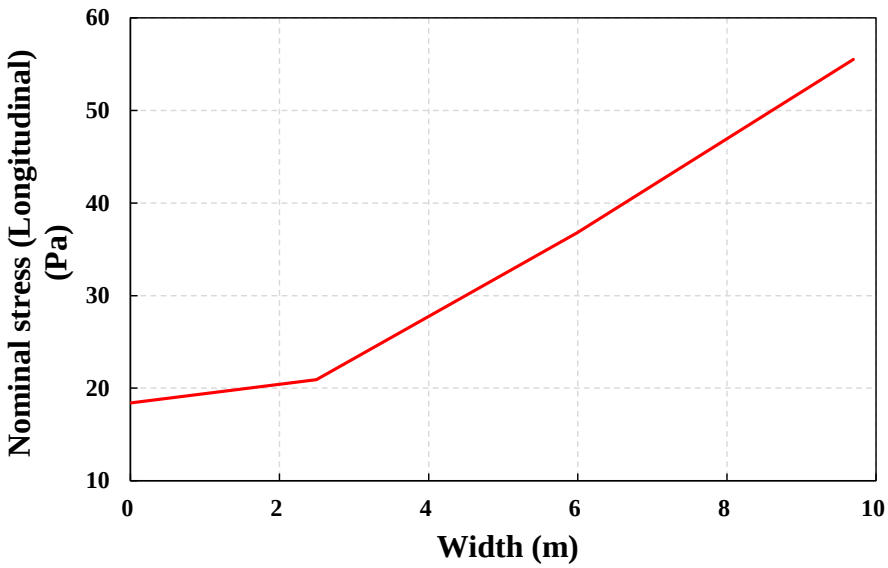
Nominal stress (Longitudinal)
(Pa)
60
50
40
30
20
10
0
2
4
6
8
10
Width (m)

(b)

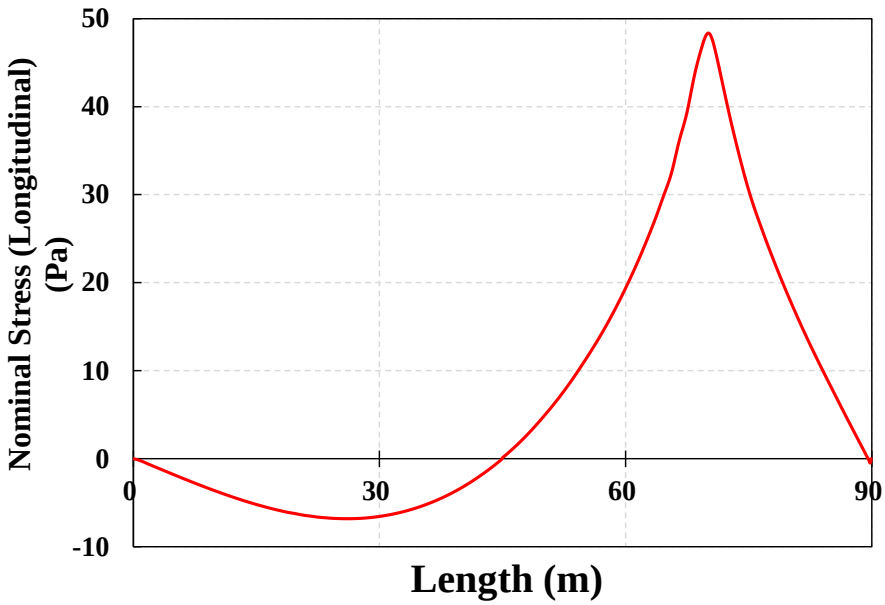

(c)

Figure 3.4. Vehicle location caused the worst load effect on fatigue-prone detail: (a) nominal stress influence surface in the longitudinal direction, (b) transversal influence line of the nominal stress at maximum stress occurrence location, (c) nominal stress influence line in the longitudinal direction

With approach 2, a time-series stress history is generated by superimposing the influence lines of multiple vehicle loads and considering all driving patterns such as entry time, driving lane, velocity, axle weights, and axle spacing of vehicles using BWIM data. Figure 3.5(a) shows the position of the vehicles along the traffic lane, and Figure 3.5(b) shows the influence lines of the nominal stress in the longitudinal direction obtained from the structural

analysis. The *ADSC* and S_{eff} were estimated using the rain-flow counting method and Miner's rule from the generated stress history. The stress spectrum was fitted as a continuous probability density function using the GMM, following the same procedure and cutoff as the strain measurement. The optimal number, weights, and parameters of the GMM components were obtained iteratively using AIC, and the fitted results were certified by the KS test. Stress ranges less than 7 MPa were excluded from the calculation. Figure 3.6 shows the stress range spectrum for the time-series stress history generated from the BWIM data and fitting results.

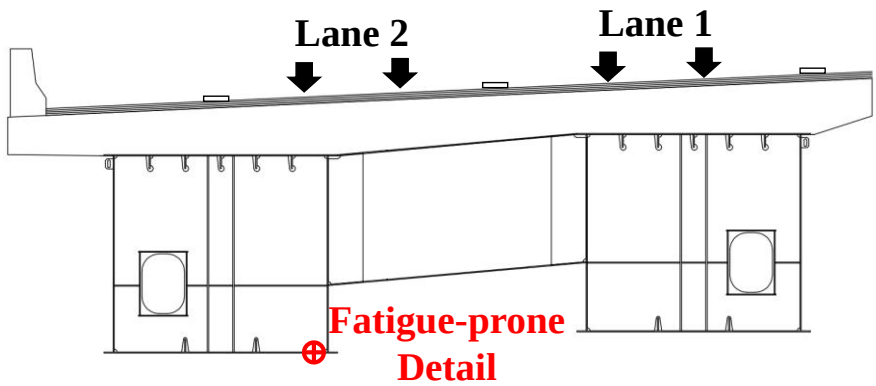

(a)

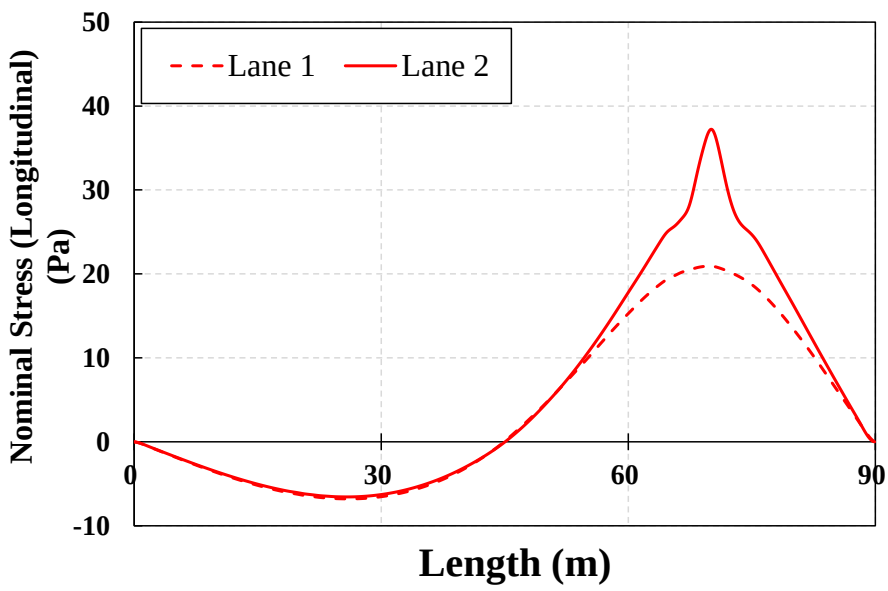

(b)

Figure 3.5 Vehicle along the traffic lane: (a) location of the vehicle, (b) nominal stress influence line at fatigue-prone detail

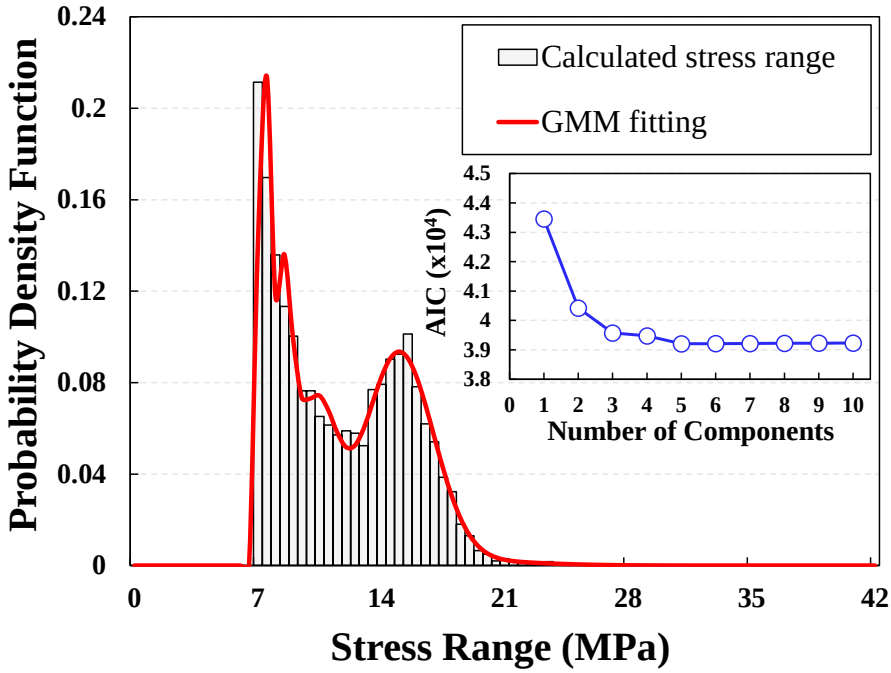

Figure 3.6 Stress range spectrum obtained from the BWIM time-series stress history

3.4 Results

Fatigue reliability analyses were performed using the strain and BWIM data. Figure 3.7 shows the results of the fatigue reliability evaluation according to the field measurement type and data-handling method. The estimated reliability index for 100 years of design life using strain measurement (β_{100yr}) was 10.42. Based on this, the fatigue life at which the fatigue reliability index of each evaluation approach equals β_{100yr} was quantitatively compared.

The fatigue life using approach 1 with BWIM data was identified as 33.8 years, and the fatigue life using approach 2 was 88.3 years. This difference in fatigue lives originates from the consideration of the driving patterns associated with the BWIM data.

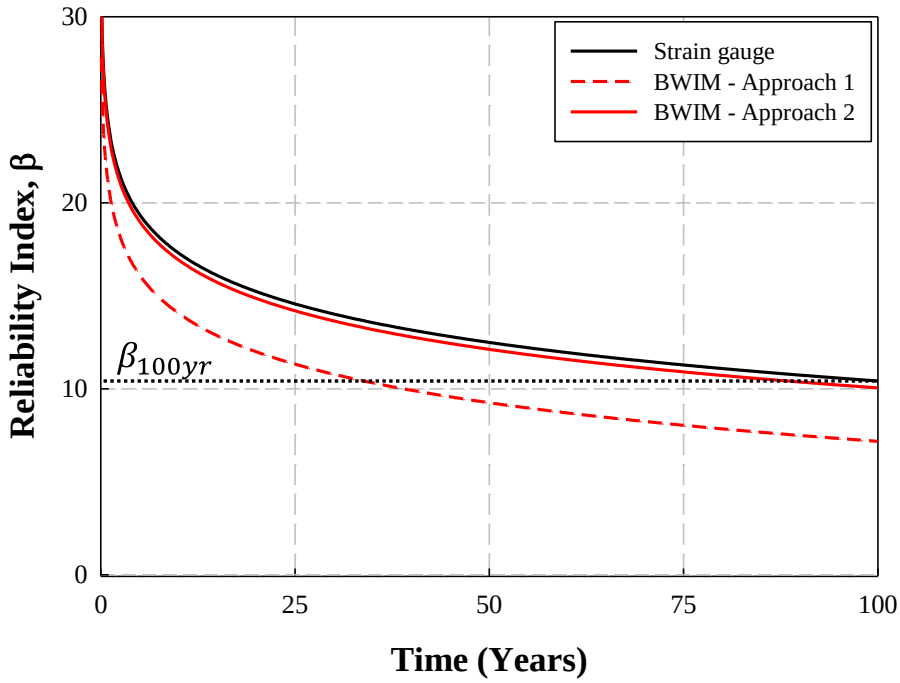

Figure 3.7 Fatigue reliability evaluation results

CHAPTER 4

Parametric Study for Driving Patterns

The driving patterns obtained from the BWIM data were identified as a critical factor in evaluating the fatigue life of the examined bridge. However, the more the driving patterns are considered, the more complex the fatigue evaluation procedure becomes. Therefore, parametric studies were conducted to identify the relative influence of each driving pattern on fatigue evaluation. The evaluation results of each case were compared with the fatigue life equal to the 100-year fatigue reliability index from the strain gauge data (β_{100yr}).

4.1 Case 1: Effect of Headway

The headway refers to the distance or time between two consecutive passing vehicles. The fatigue evaluation was based on the time-series stress history to which the headway was applied; the entry time and driving speed among the driving patterns were also considered. If the vehicles are located in the same span, the fatigue damage is evaluated to be greater owing to the superposition of vehicle loads. In other words, according to the S-N curve, the fatigue life decreased to the cube of the rate of load increase. Therefore, case 1, which additionally considered the headway in approach 1, evaluated

a larger stress range. As the stress range increased, the number of stress range cycles above the cutoff increased. Figure 4.1 shows the stress range spectrum and fitting results, and the evaluated fatigue reliability index is shown in Figure 4.2. However, in the case of the target bridge, only 8.5% of the total heavy vehicle volume was located within the same span, owing to the limited length of the bridge. It implied that with case 1, which additionally considered the headway in approach 1, the fatigue life was slightly reduced from 33.8 years to 30.1 years. This confirms that the influence of the headway is insignificant for the fatigue evaluation of bridges with a relatively short-to-medium span.

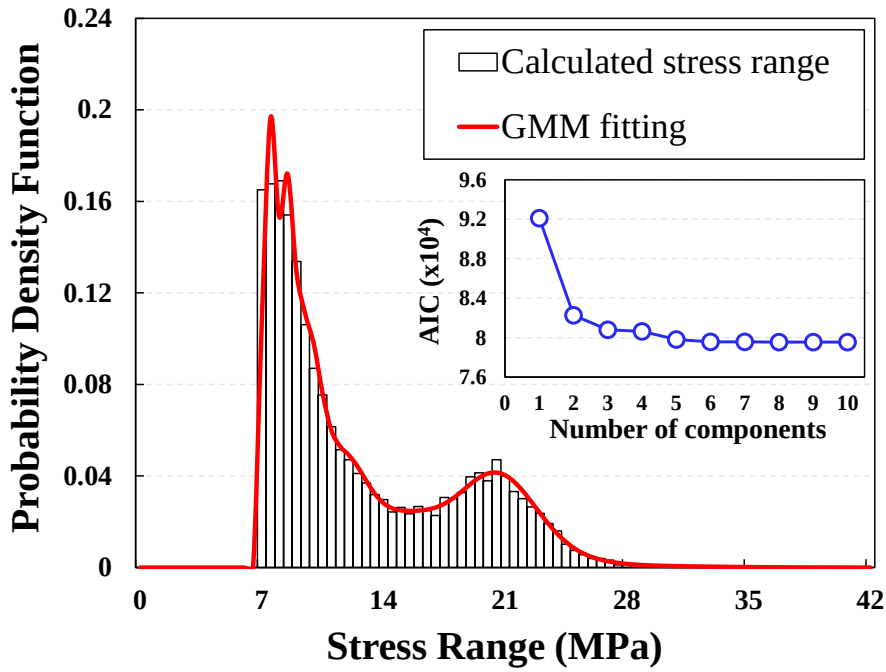

Figure 4.1 Stress range spectrum obtained from BWIM data: Case 1

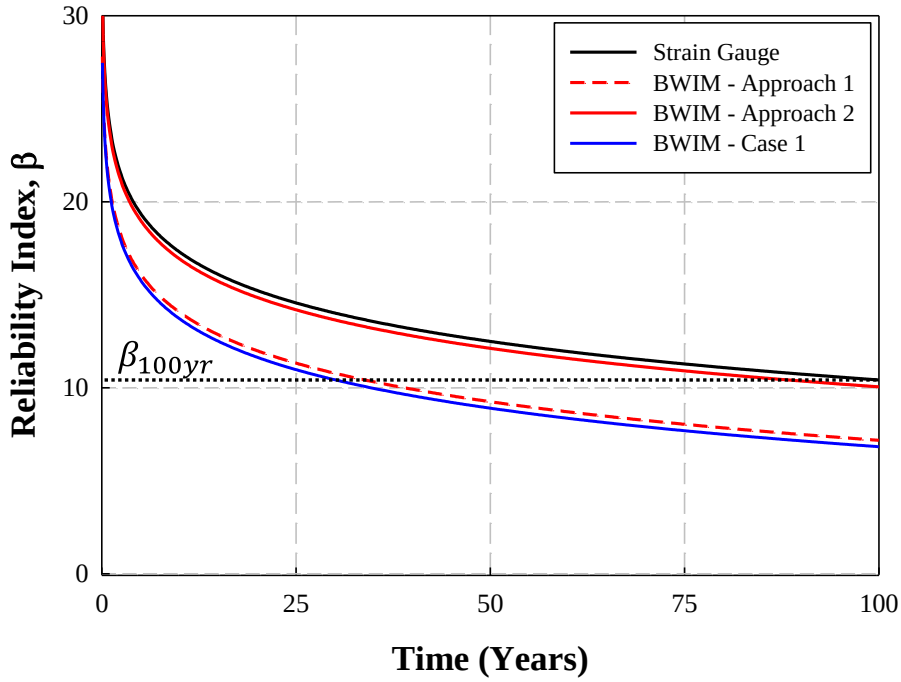

Figure 4.2 Fatigue reliability evaluation result: Case 1

4.2 Case 2: Effect of Driving Lane

Even with the same vehicle load, the stress applied to a fatigue-prone detail varies depending on the transverse position of the vehicle load, as shown in Fig. 8b. The stress range can be reduced compared to the worst load effect when the vehicles are separated into each traffic lane. As the stress range decreased, the number of stress range cycles above the cutoff decreased. Figure 4.3 shows the stress range spectrum and fitting results. The fatigue reliability index evaluated based on this is shown in Figure 4.4. The fatigue life evaluated by case 2, which additionally considers the driving lanes of

approach 1, was significantly increased from 33.8 years to 66.2 years. Therefore, the influence of driving lanes is considered a significant aspect of the fatigue evaluation of bridges.

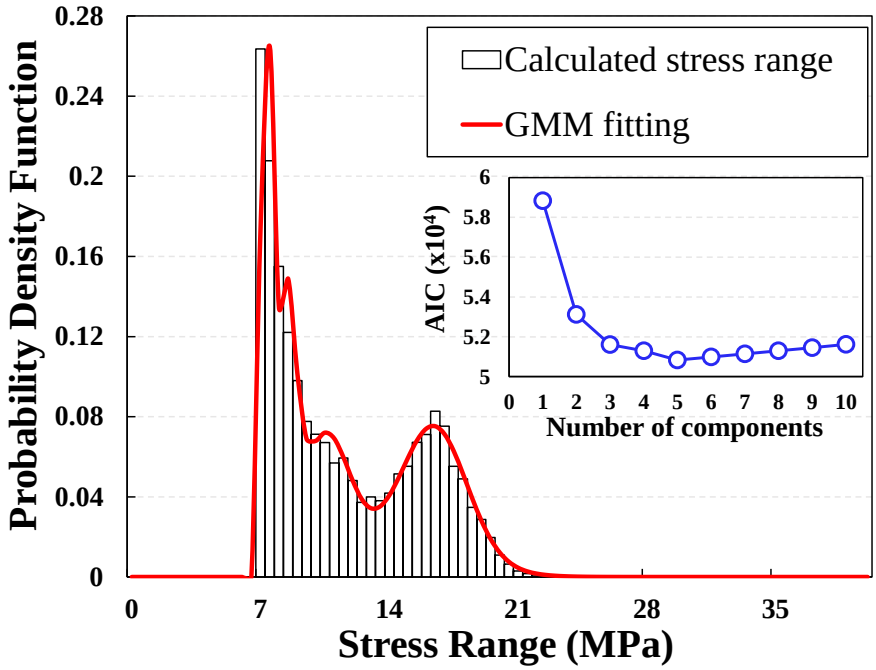

Figure 4.3 Stress range spectrum obtained from BWIM data: Case 2

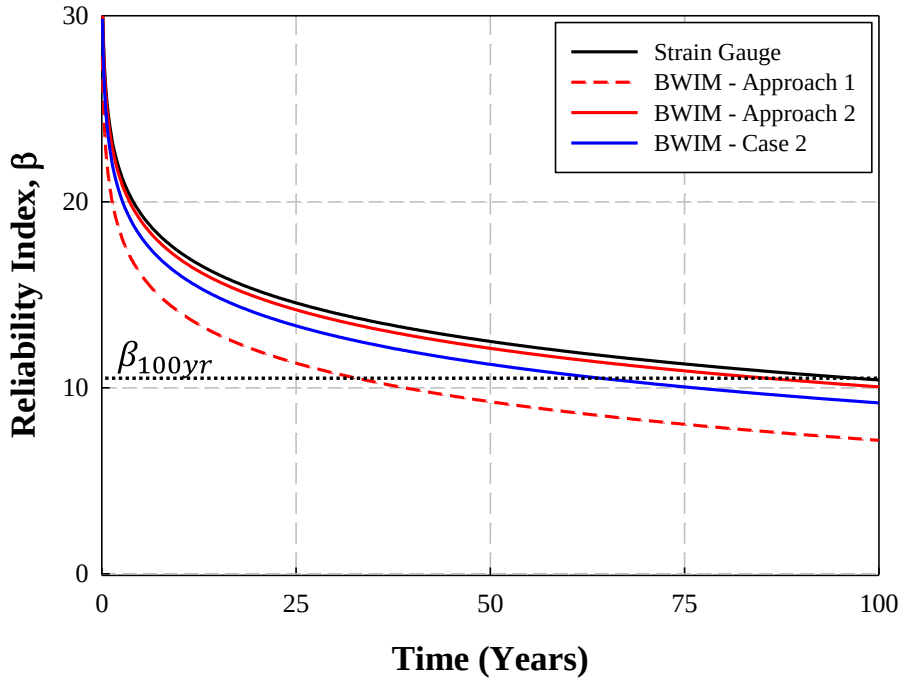

Figure 4.4 Fatigue reliability evaluation result: Case 2

4.3 Case 3: Effect of Axle Load Distribution

The axle load distribution considers vehicle weight rather than the number of wheel axles. The stress range applied to the fatigue-prone detail is reduced when the vehicle weight is considered the load distribution on the axles compared with the GVW. In addition, the influence of the axle-load distribution became more dominant for bridges with short spans. Case 3 considers the load distributed by the axles instead of the GVW used in approach 1. Figure 4.5 shows the stress range spectrum and fitting results. The fatigue reliability index evaluated based on this is shown in Figure 4.6.

The fatigue life increased from 33.8 years to 46.9 years because the stress range evaluated in case 3 was reduced. Therefore, the influence of the axle load distribution is confirmed to be essential for the fatigue evaluation of bridges with short-to-medium spans.

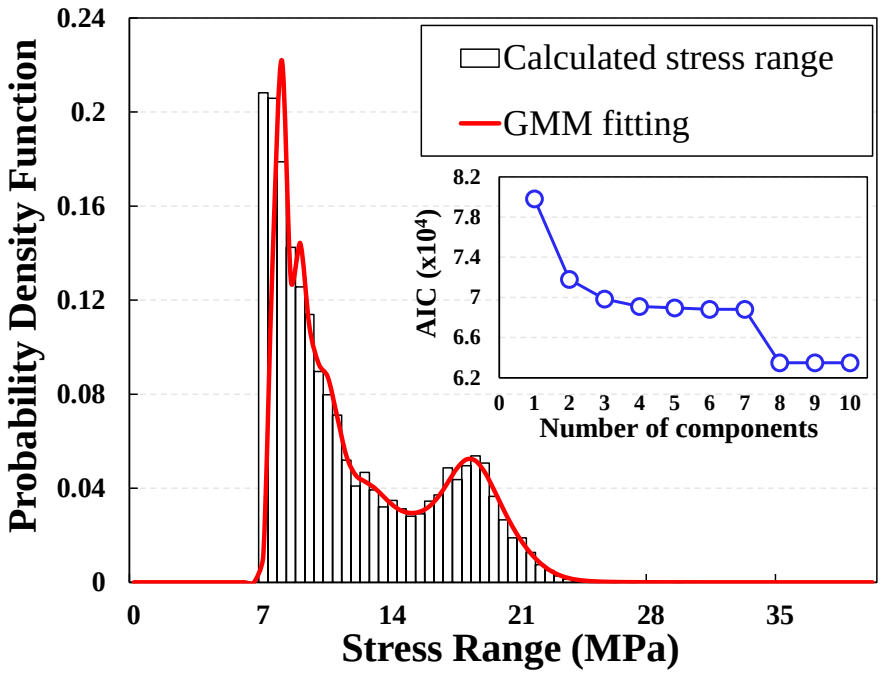

Figure 4.5 Stress range spectrum obtained from BWIM data: Case 3

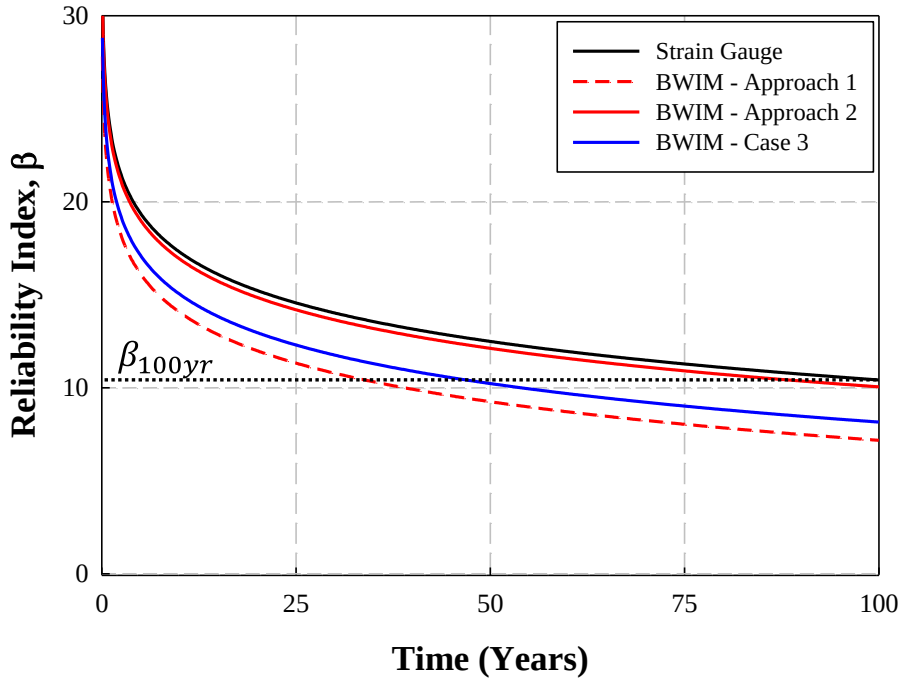

Figure 4.6 Fatigue reliability evaluation result: Case 3

4.4 Case 4: Two Driving Patterns

Based on the results of cases 1 to 3, the fatigue reliability evaluation was performed by considering the driving patterns while excluding the relatively minor influence of the headway. When calculating the stress range, the influence line for each traffic lane was used and overlapped by considering the axle weight and spacing. Because the headway of vehicles was not considered, the stress ranges applied to the fatigue-prone detail for each vehicle were encountered separately. Figure 4.7 shows the stress range spectrum and fitting results, and the fatigue reliability index evaluated based

on this is shown in Figure 4.8. In case 4, the fatigue life was significantly increased from 33.8 years to 95.8 years. Therefore, when evaluating the fatigue life of steel bridges with short-to-medium spans, approach 2 is feasible even when only the factors of the driving lane, axle weight, and axle spacing are considered.

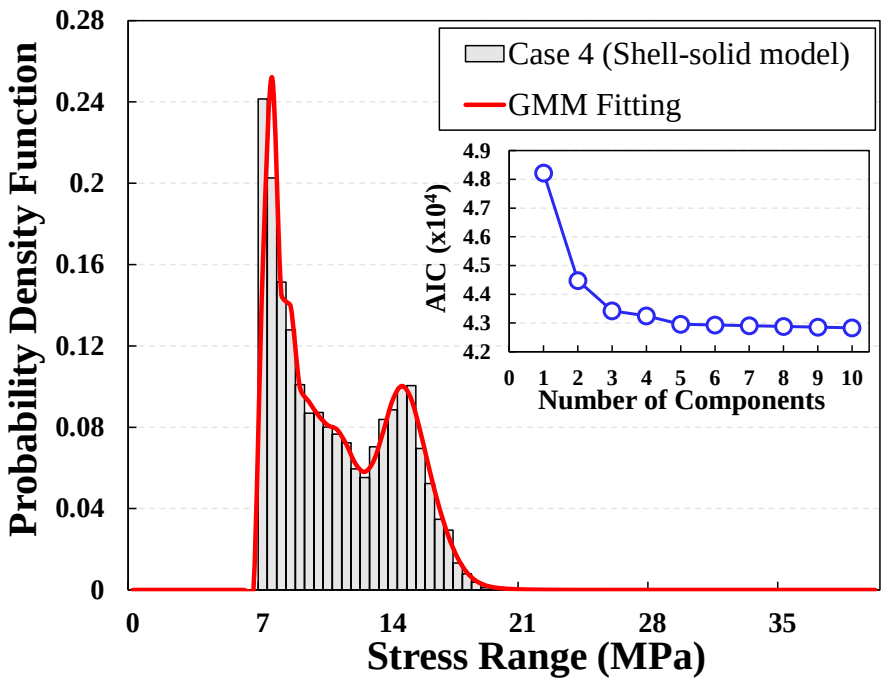

Figure 4.7 Stress range spectrum obtained from BWIM data: Case 4

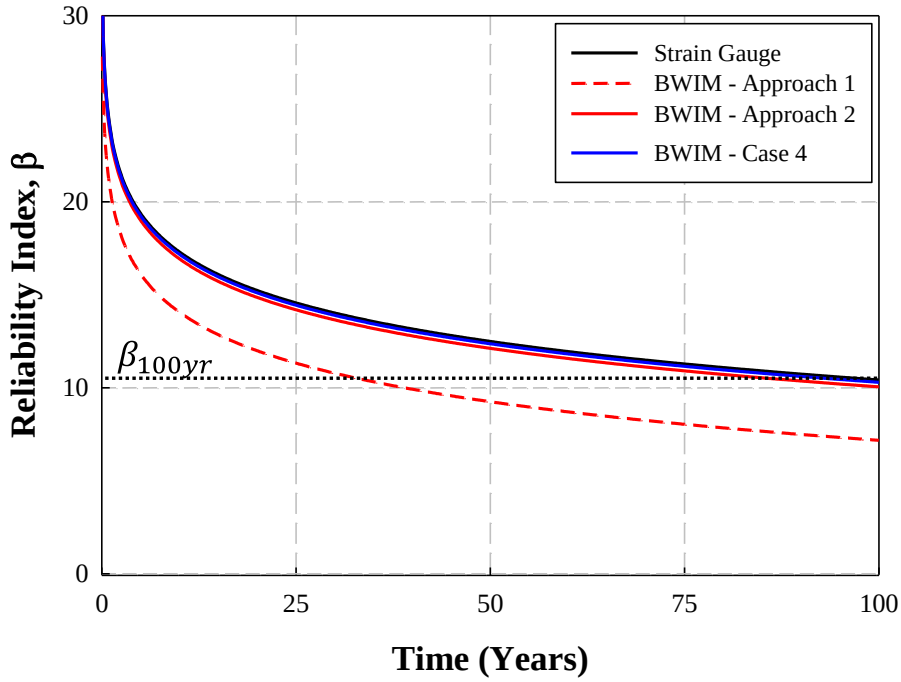

Figure 4.8 Fatigue reliability evaluation result: Case 4

4.5 Summary of Parametric Study

The considerations of the driving patterns and the results of the fatigue evaluation for each parametric study case, which includes the two approaches described in Chapter 3, are summarized in Table 4.1. The estimated fatigue reliability indices in terms of the service life are shown in Figure 4.9.

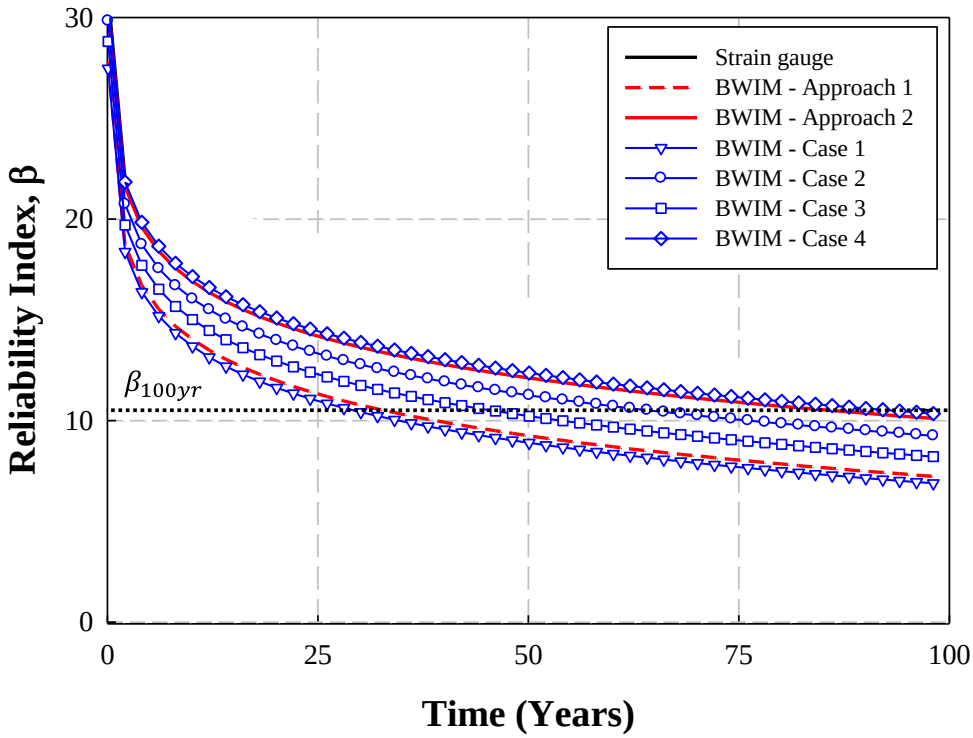

Figure 4.9 Evaluated Fatigue Reliability Indices

Table 4.1 Parametric study cases and evaluated fatigue lives

Parametric study cases	BWIM-measured driving patterns				Fatigue life (year)
	GVW	Entry time and driving speed	Driving lane	Axle weights and spacing	
Approach 1 (only GVW)	O				33.8
Approach 2 (all driving patterns)		O	O	O	88.3
Case 1 (headway)	O	O			30.1
Case 2 (driving lane)	O		O		66.2
Case 3 (axle load distribution)				O	46.9
Case 4 (two driving patterns)			O	O	95.8

CHAPTER 5

Conclusions

In this study, fatigue reliability evaluations were performed using strain gauges and BWIM data measured during the same period on an in-service steel bridge.

(1) To confirm the effect of the accuracy of the structural analysis models on fatigue evaluation using BWIM data, a frame model and a shell-solid model of the target bridge were generated using commercial structural analysis programs. The single vehicle cases were selected from the BWIM data to validate the analysis models. The same vehicle load was applied to the analysis model and compared with the strain measurement at the coincident time. As a result of comparing 1,561 cases to the stress range from strain gauge data, the nominal stress range calculated using BWIM and structural analysis models was 12% and 4% larger on average when using the frame model and the shell-solid model, respectively.

(2) The approaches that use a GVW spectrum and a time-series stress history to consider the driving patterns were investigated. Fatigue reliability evaluations were performed according to each approach

using the shell-solid model. Based on the design-life-fatigue reliability index, β_{100yr}, of strain measurement, the fatigue life in which the fatigue reliability index of each evaluation approach equaled β_{100yr} was quantitatively compared. As a result, the fatigue reliability evaluations of the fatigue life by approach 1 were three times shorter. In contrast, evaluations of fatigue life by approach 2 were 1.1 times shorter. The consideration of driving patterns using BWIM data had a significant influence on fatigue damage evaluation. Therefore, the results of this study suggest that driving patterns should be considered for the accurate fatigue life evaluation of steel bridges.

(3) For the fatigue life evaluation, parametric studies were conducted on the effect of each BWIM-measured driving pattern: entry time, driving speed, driving lane, axle weights, and spacing. In particular, the influence of the headway was relatively insignificant because vehicles were rarely located within the same span. In other words, the influences of the axle load distribution and driving lane were dominant for evaluating steel bridges with short spans. Therefore, the results of this study confirmed that it is possible to conduct an accurate strain measurement using a method similar to approach 2 and considering only the driving lane, axle weight, and axle spacing.

REFERENCE

AASHTO. (2018). *AASHTO The Manual for Bridge Evaluation.* American Association of State Highway and Transportation Officials (AASHTO). Washington, DC.

AASHTO. (2020). *AASHTO LRFD Bridge Design Specification.* American Association of State Highway and Transportation Officials (AASHTO). Washington, DC.

Akaike, H. (1974). New Look at Statistical-Model Identification. *Ieee Transactions on Automatic Control*, Ac19(6), 716-723.

Alencar, G., Hong, J.K., de Jesus, A., da Silva, J.G.S., and Calcada, R. (2021). The Master S-N curve approach for fatigue assessment of welded bridge structural details. *International Journal of Fatigue*, 152

Chotickai, P. and Bowman, M.D. (2006). Truck Models for Improved Fatigue Life Predictions of Steel Bridges. *Journal of Bridge Engineering*, 11(1), 71-80.

Chung, H.Y. (2004). *Fatigue Reliability and Optimal Inspection Strategies for Steel Bridges*. Dissertation, Civil and Environmental Engineering Department, The University of Texas at Austin, Austin, TX.

Connor, R.J., Fisher, J.W., Hodgson, I.C., and Bowman, C.A. (2004). *Results of Field Monitoring Prototype Floorbeam Connection Retrofit Details on the Birmingham Bridge.* ATLSS Report, No. 04-04, Lehigh University's Center for Advanced Technology for Large Structural Systems (ATLSS), Bethlehem, PA.

Connor, R.J., Hodgson, I.C., Mahmoud, H.N., and Bowman, C.A. (2005). *Field Testing and Fatigue Evaluation of the I-29 Neville Island Bridge over the Ohio River.* ATLSS Report, No. 05-02, Lehigh University's Center for Advanced Technology for Large Structural Systems (ATLSS), Bethlehem, PA.

Dassault Systems. (2021). *ABAQUS 2021*. Providence, RI: Dassault Systemes Simulia Corp.

Deng, Y., Li, A.Q., and Feng, D.M. (2018). Fatigue Reliability Assessment for Orthotropic Steel Decks Based on Long-Term Strain Monitoring. *Sensors*, 18(1), 181.

Deng, Y., Zhang, M., Feng, D.M., and Li, A.Q. (2021). Predicting fatigue damage of highway suspension bridge hangers using weigh-in-motion data and machine learning. *Structure and Infrastructure Engineering*, 17(2), 233-248.

Downing, S.D. and Socie, D.F. (1982). Simple Rainflow Counting Algorithms. *International Journal of Fatigue*, 4(1), 31-40.

Fisher, J.W., Kulak, G.L., and Smith, I.F.C. (1998). *A Fatigue Primer for Structural Engineers*. National Steel Bridge Alliance, U.S.A.

Fisher, J.W. and Roy, S. (2011). Fatigue of steel bridge infrastructure. *Structure and Infrastructure Engineering*, 7(8), 457-475.

Frangopol, D.M., Strauss, A., and Kim, S. (2008). Bridge reliability assessment based on monitoring. *Journal of Bridge Engineering*, 13(3), 258-270.

Guo, T., Frangopol, D.M., and Chen, Y.W. (2012). Fatigue reliability assessment of steel bridge details integrating weigh-in-motion data and probabilistic finite element analysis. *Computers & Structures*, 112245-257.

Hobbacher, A.F. (2009). The new IIW recommendations for fatigue assessment of welded joints and components - A comprehensive code recently updated. *International Journal of Fatigue*, 31(1), 50-58.

Hodgson, I.C., Connor, R.J., Mahmoud, H.N., and Bowman, C. (2006). *Approaches to the Fort Duquesne Bridge Retrofit of Fatigue and Fracture Details.* ATLSS Report, No. 06-06, Lehigh University's Center for Advanced Technology for Large Structural Systems (ATLSS), Bethlehem, PA.

Iatsko, O., Babu, A.R., Stallings, J.M., and Nowak, A.S. (2020). Weigh-in-Motion-Based Fatigue Damage Assessment. *Transportation Research Record*, 2674(8), 710-719.

Kawada, Y. and Misawa, H. (1968). The effect of stress amplitudes below endurance limit on the cumulative fatigue life. *Journal of Society of Materials Science of Japan*, 17(173), 123-127.

Keating, P.B. and Fisher, J.W. (1986). *Evaluation of FatigueTests and Design Criteria on Welded Details.* NCHRP Report, No. 286, Transportation Research Board, Washington, DC.

Kim, J. and Song, J. (2019). A Comprehensive Probabilistic Model of Traffic Loads based on Weigh-in-Motion Data for Applications to Bridge Structures. *Ksce Journal of Civil Engineering*, 23(8), 3628-3643.

Kwon, K. and Frangopol, D.M. (2010). Bridge fatigue reliability assessment using probability density functions of equivalent stress range based on field monitoring data. *International Journal of Fatigue*, 32(8), 1221-1232.

Kwon, K., Frangopol, D.M., and Soliman, M. (2012). Probabilistic Fatigue Life Estimation of Steel Bridges by Using a Bilinear S-N Approach. *Journal of Bridge Engineering*, 17(1), 58-70.

Liu, Y., Xiao, X.H., Lu, N.W., and Deng, Y. (2016). Fatigue Reliability Assessment of Orthotropic Bridge Decks under Stochastic Truck Loading. *Shock and Vibration*, 2016

Lu, N.W., Liu, Y., and Deng, Y. (2019). Fatigue Reliability Evaluation of Orthotropic Steel Bridge Decks Based on Site-Specific Weigh-in-Motion Measurements. *International Journal of Steel Structures*, 19(1), 181-192.

Lu, N.W., Noori, M., and Liu, Y. (2017). Fatigue Reliability Assessment of Welded Steel Bridge Decks under Stochastic Truck Loads via Machine Learning. *Journal of Bridge Engineering*, 22(1),

Mao, J.X., Wang, H., and Li, J. (2019). Fatigue Reliability Assessment of a Long-Span Cable-Stayed Bridge Based on One-Year Monitoring Strain Data. *Journal of Bridge Engineering*, 24(1), 05018015.

Midas IT. (2021). *MIDAS Civil 2021*. Providence, RI: MIDAS Information Technology Corp.

Miner, M.A. (1945). Cumulative Damage in Fatigue. *Journal of Applied Mechanics-Transactions of the Asme*, 12(3), 159-164.

MOLIT. (2016). *Korean Highway Bridge Design Code (Limit State Design Method).* Ministry of Land, Infrastructure, and Transport (MOLIT). Sejong-si.

Moses, F., Schilling, C.G., and Raju, K.S. (1987). *Fatigue Evaluation Procesdures for Steel Bridges.* NCHRP Report, No. 299, Transportation Research Board, Washington, DC.

Murakami, Y., Takagi, T., Wada, K., and Matsunaga, H. (2021). Essential structure of S-N curve: Prediction of fatigue life and fatigue limit of defective materials and nature of scatter. *International Journal of Fatigue*, 146

Ni, Y.Q., Ye, X.W., and Ko, J.M. (2010). Monitoring-Based Fatigue Reliability Assessment of Steel Bridges: Analytical Model and Application. *Journal of Structural Engineering*, 136(12), 1563-1573.

Ni, Y.Q., Ye, X.W., and Ko, J.M. (2012). Modeling of Stress Spectrum Using Long-Term Monitoring Data and Finite Mixture Distributions. *Journal of Engineering Mechanics*, 138(2), 175-183.

Nyman, W.E. and Moses, F. (1985). Calibration of Bridge Fatigue Design-Model. *Journal of Structural Engineering-Asce*, 111(6), 1251-1266.

Shin, D.K., Kwon, T.H., and Park, Y.S. (2007). Reliability Analysis of Fatigue Truck Model Using Measured Truck Traffic Statistics. *Journal of Korean Society of Steel Construction*, 19(2), 211-221.

Sivakumar, B., Ghosn, M., and Moses, F. (2011). *Protocols for Collecting and Using Traffic Data in Bridge Design.* NCHRP Report, No. 683, Transportation Research Board, Washington, DC.

Wirsching, P.H. (1984). Fatigue Reliability for Offshore Structures. *Journal of Structural Engineering*, 110(10), 2340-2356.

Yan, D.H., Luo, Y., Lu, N.W., Yuan, M., and Beer, M. (2017). Fatigue Stress Spectra and Reliability Evaluation of Short- to Medium-Span Bridges under Stochastic and Dynamic Traffic Loads. *Journal of Bridge Engineering*, 22(12),

Yan, D.H., Luo, Y., Yuan, M., and Lu, N.W. (2017). Lifetime fatigue reliability evaluation of short to medium span bridges under site-specific stochastic truck loading. *Advances in Mechanical Engineering*, 9(3),

Yen, B.T., Hodgson, I.C., Zhou, E., and Crudele, B.B. (2009). *Estimation of Fatigue Life below CAFL* 2nd International Conference on Fatigue and Fracture in the Infrastructure, Bethlehem, PA.

APPENDIX

A. Information of Bridge Members

A.1 Steel box girder

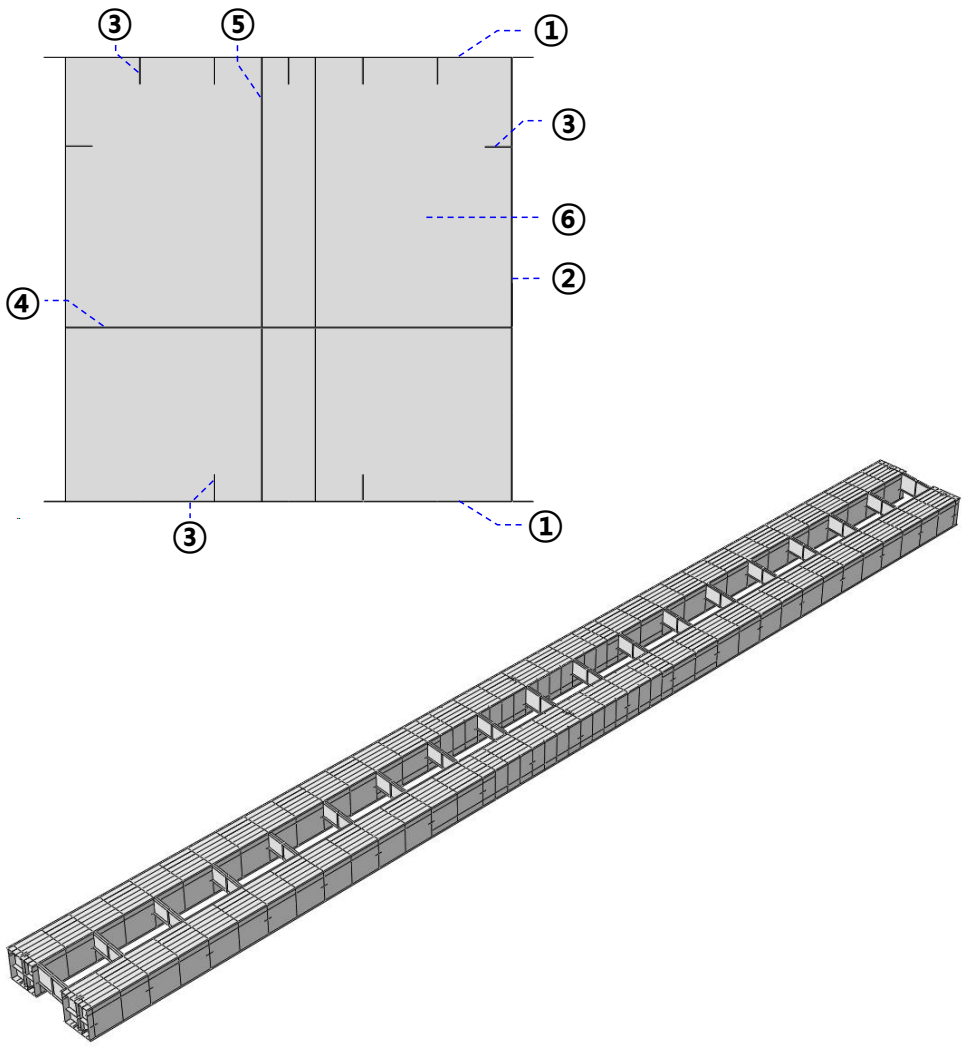

Figure A. 1 Steel box girder

Table A. 1 Information of steel box girder member

Bridge element		t (mm)	Steel grade
① Top/bottom flange		14	SM490A*
② Web		12	SM490A*
③ Top/bottom longitudinal rib		12	SM400A**
④ Horizontal stiffner		12	SM400A**
⑤ Vertical stiffener	Support	20	SM490A*
	Else	12	SM400A**
⑥ Diaphragm	Middle support	20	SM490A*
	End support	12	SM490A*
	Else	12	SM400A**

* SM490A: $F_{u.min}$ = 490MPa

** SM400A: $F_{u.min}$ = 400MPa

A.2 Crossbeam

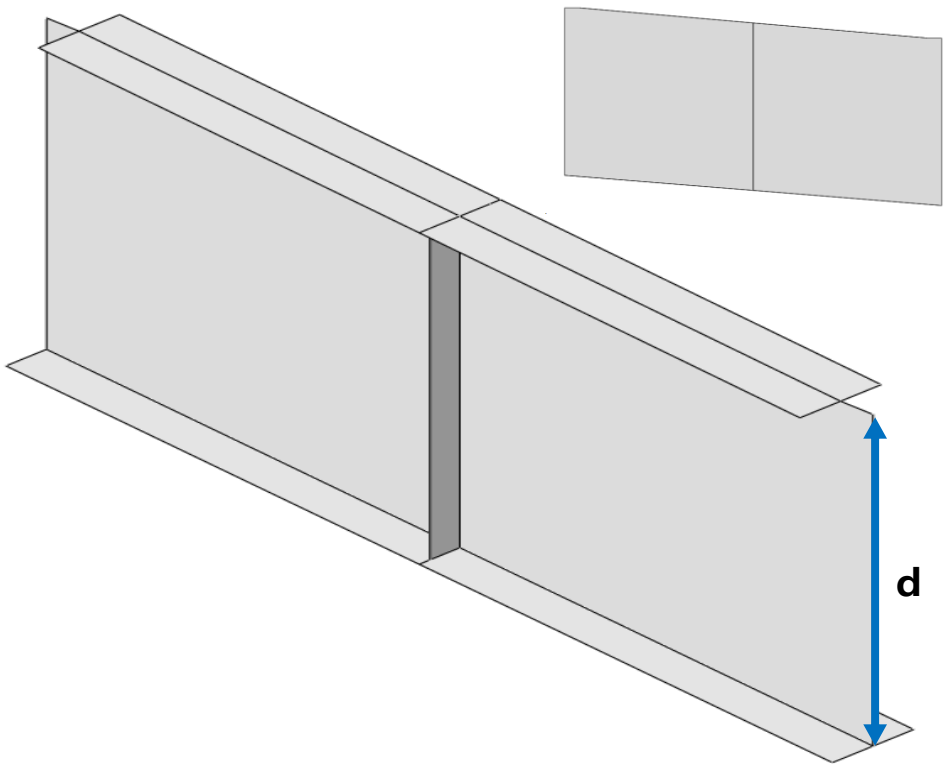

Figure A. 2 Crossbeam

Table A. 2 Information of cross beam member

Bridge element		d (mm)	t (mm)	Steel grade
Crossbeam	Support	1500	12	SM490A*
	Else	1250	12	SM400A**

* SM490A: $F_{u.min}$ = 490MPa

** SM400A: $F_{u.min}$ = 400MPa

A.3 Concrete slab

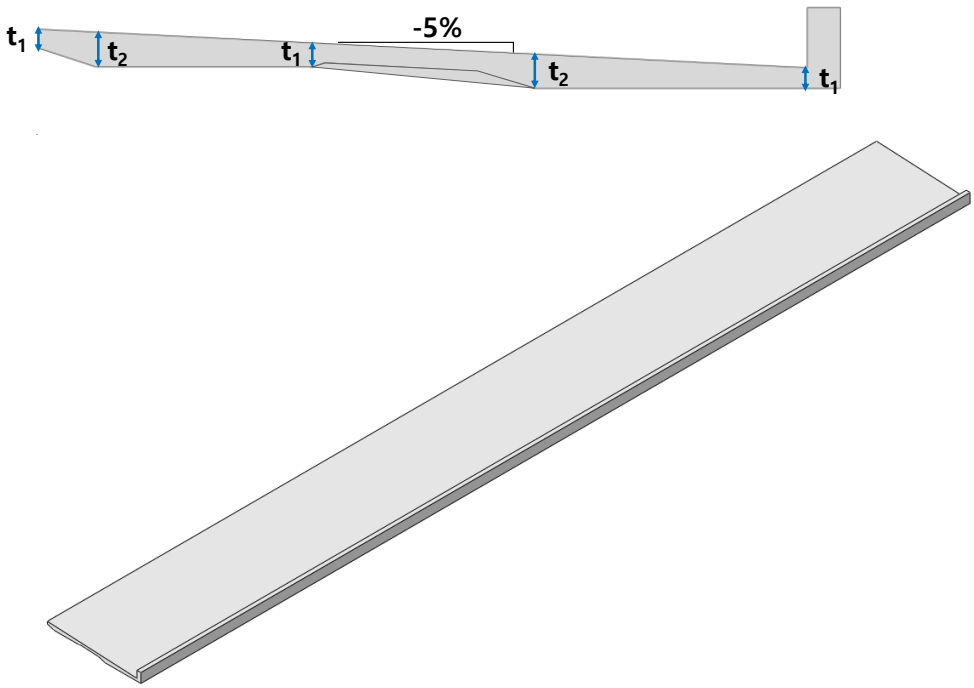

Figure A. 3 Concrete slab

Table A. 3 Information of concrete slab

Bridge element	t_1 (mm)	t_2 (mm)	Mass density (ton/m^3)	Young's modulus (MPa)	Poisson's ratio
Concrete slab	240	750	2500	24500	0.167

국 문 초 록

이상현

건설환경공학부

서울대학교 대학원

이 연구에서는 현장계측된 변형률 및 BWIM 데이터를 활용한 공용 중 강 교량의 피로수명을 확률론적으로 평가하는 전반적인 절차 및 방법에 대해 검토하였다.

현장계측의 종류에 따른 피로 신뢰도 평가 결과의 차이를 정량적으로 검토하기 위해 실제 공용 중인 강 교량에서 동일한 기간동안 변형률 및 BWIM 계측을 수행하였다. 또한, BWIM 데이터를 활용한 피로 평가 시 활용되는 구조해석모델의 정밀성이 평가 결과에 미치는 영향에 대해 확인하기 위해, 뼈대구조요소 단순해석모델과 유한요소 상세해석모델을 각각 상용 구조해석 프로그램을 이용하여 구축하였다.

선행연구 조사 결과들을 바탕으로, BWIM 데이터와 구조해석모델을 활용하여 교량 부재의 피로 취약 상세에 가해지는 유효응력범위 및 반복응력횟수를 추정하는 두 가지 처리 기법을 정의하였다. 일반적으로 가장 정확한 평가 방법으로 인식되는 변형률 계측 데이터를 활용한 방법을 기준으로, 두 BWIM 데이터 처리 기법에 따른 피로 신뢰도 평가 결과를 비교하였다. 비교된 피로 신뢰도 평가 결과를 통해 BWIM 데이터 처리 시 고려되는 주행 패턴들이 평가 피로 수명에 큰 영향을 미침을 확인하였다.

마지막으로, BWIM 데이터로부터 고려될 수 있는 대표적인 3가지 주행 패턴(연행 효과, 주행 차선, 축 하중 분산)을 정의하고, 각 주행 패턴이 평가 결과에 미치는 영향에 대한 검토를 수행하였다. 평가 대상 교량과 같은 일반적인 단-중 경간의 강 교량의 경우, 차량 하중의 연행에 의한 동시 재하보다는 차량의 주행 차선 및 차축에 의한 하중 분산 효과가 교량의 피로 수명을 평가하는데 있어 보다 지배적인 영향을 미치며, 이 두 가지 주행 패턴만을 고려하더라도 변형률 데이터에 의한 평가 결과만큼 충분히 정확한 피로 수명의 평가가 가능함을 확인하였다.

주요어: 강 교량, 피로, 신뢰도 평가, 현장 계측, 변형률, Bridge weigh-in-motion (BWIM), 유한요소모델

학번: 2020-22553

공학석사학위논문

Fatigue Reliability Evaluation of In-service Steel Bridge Using Measured Strain and BWIM Data

변형률 및 BWIM 계측 데이터를 활용한 공용 중 강 교량의 피로 신뢰도 평가

2022 년 2 월

서울대학교 대학원

건설환경공학부

이 상 현

Fatigue Reliability Evaluation of In-service Steel Bridge Using Measured Strain and BWIM Data

변형률 및 BWIM 계측 데이터를 활용한 공용 중 강 교량의 피로 신뢰도 평가

지도교수 김 호 경

이 논문을 공학석사 학위논문으로 제출함

2022년 2월

서울대학교 대학원

건설환경공학부

이 상 현

이상현의 공학석사 학위논문을 인준함

2021년 12월

위 원 장		(인)
부 위 원 장		(인)
위 원		(인)

ABSTRACT

Fatigue Reliability Evaluation of In-service Steel Bridge Using Measured Strain and BWIM Data

Sang Hyeon Lee

Department of Civil and Environmental Engineering

Seoul National University

Strain gauges and bridge weigh-in-motion (BWIM) are representative field measurements normally used for the fatigue evaluation of in-service steel bridges. To evaluate the reliability of fatigue damage accumulation, the effective stress range and number of stress cycles applied to fatigue-prone details should be estimated based on field-measured data of a target bridge. However, the procedure for using field measurements to estimate either the effective stress range or the number of stress cycles has not been explicitly presented. Furthermore, studies that have quantitatively compared the differences in fatigue evaluation results according to the field measurement type or BWIM data-processing techniques are still insufficient. In this study, the strain and BWIM data were measured simultaneously on an in-service steel bridge to evaluate the fatigue damage. Both a frame model and a shell-solid model were used to examine the accuracy of the structural analysis models when using BWIM data. Two approaches using BWIM data to

estimate effective stress and average daily stress cycles were investigated. In addition, parametric studies have been conducted on the effect of driving patterns on fatigue evaluation. The differences in the fatigue evaluation results based on the type of field measurement and driving patterns were quantitatively compared. As a result, the fatigue reliability evaluation could be sufficiently accurate even when only two dominant driving patterns were used for steel bridges with typical short-to-medium spans.

Keywords: Steel bridge, Fatigue, Reliability Evaluation, Field test, Strain, Bridge weigh-in-motion (BWIM), Finite element model

Student Number: 2020-22553

TABLE OF CONTENTS

LIST OF FIGURES

LIST OF TABLES

CHAPTER 1

INTRODUCTION

1.1 Research Background

Fatigue in steel is a process of initiation and growth of cracks under numerous repetitive loads. This process can occur at stress levels that are substantially lower than those associated with failure under static loading conditions. The most common civil engineering structures that must be examined for fatigue are bridges (Fisher et al., 1998).

As the service life of a bridge increases, fatigue damage continues to accumulate owing to the repetitive stress range generated on the bridge members when vehicles pass. Figure 1.1 shows examples of fatigue cracks in steel bridges reported in a precedent study (Fisher and Roy, 2011).

Figure 1.1 Fatigue cracks in steel bridge (Fisher and Roy, 2011)

Because the accumulation of fatigue damage can cause the failure of bridge members, a quantitative evaluation is necessary to ensure the safety of a bridge (Nyman and Moses, 1985; Chotickai and Bowman, 2006). AASHTO LRFD (AASHTO, 2020) classified welded and bolted details for steel bridges into categories A to E' according to the connected shape and stress direction of the bridge members. According to the category of fatigue-prone details of the target bridge, the fatigue life of the bridge can be evaluated based on the design S-N curve. The relationship between the nominal stress range and the number of stress cycles of the design S-N curve was determined from the experimental results obtained under constant-amplitude loading. Therefore, when evaluating the fatigue life of a bridge based on the design S-N curve, it is necessary to exclude the local stress concentration and convert the variable-amplitude stress range of the measured stress history into an equivalent constant-amplitude stress range.

1.2 Fatigue Evaluation Using Field-measured Data

Determining the repetitive stress range and the number of stress cycles is a vital task in fatigue evaluation. The repetitive stress range applied to bridge members can be evaluated using either the strain data of the fatigue-prone detail or the cumulative weights of the vehicles passing through the bridge measured via the bridge weigh-in-motion (BWIM). The number of stress

cycles was calculated from the stress spectrum, and the variable-amplitude stress range histogram can be converted into an equal number of constant-amplitude stress range histogram according to Miner's rule (Miner, 1945).

Fatigue evaluation using strain data is generally considered the most accurate approach (AASHTO, 2018). Various fatigue reliability evaluation methods have been proposed for applying the randomness of strain measurements as a probability distribution. Frangopol et al. (2008) proposed a method to evaluate the fatigue damage of in-service steel bridges by considering the uncertainty of field measurements. Kwon and Frangopol (2010) considered the variability in the effective stress range based on the cutoff change in the stress range. Deng et al. (2018) considered the daily variability in the effective stress range based on strain data gathered from long-term measurements. Mao et al. (2019) considered the monthly variability in the effective stress range and number of stress cycles from long-term measurements of strain data. In particular, if the data are insufficient owing to a short measurement period, it is necessary to consider the uncertainty by fitting the stress range spectrum to a continuous probability density function (Ni et al., 2010; 2012).

However, it is sometimes difficult to install strain gauges on fatigue-prone details, owing to rivets or welding. Installing strain gauges on all fatigue-prone details of bridges makes it unreasonable in terms of maintenance costs.

To solve these limitations, several studies have been conducted to probabilistically evaluate the fatigue damage of in-service steel bridges using BWIM data and structural analysis models of bridges instead of strain data. Fatigue reliability evaluations are performed by positioning vehicle loads based on a probabilistic model of axle loads and spacing as measured by BWIM along driving lanes (Guo et al., 2012), or on fatigue-prone details that demonstrate the worst load effects (Liu et al., 2016; Lu et al., 2017; Lu et al., 2019). In addition, fatigue reliability is evaluated using a time-series stress history that considers input from multiple presences from the lanes and vehicle speeds to calculate the stress spectrum (Yan, Luo, Lu, et al., 2017; Yan, Luo, Yuan, et al., 2017; Deng et al., 2021).

However, the driving patterns and accuracy of the structural analysis models were different for each study because the fatigue evaluation procedure for using BWIM data or structural analysis modelling was not specified in the evaluation manual. In addition, studies that have quantitatively compared the differences in fatigue evaluation results according to the type of field measurement, accuracy of the structural analysis model, and consideration of driving patterns are still insufficient.

1.3 Research Objective and Scope

This study presents a suggestion for using the available BWIM data from

a complete field experiment to produce a more reliable fatigue assessment of steel bridges with short-to-medium spans. The driving patterns considered in performing fatigue reliability evaluations can significantly affect the calculated fatigue life of the target bridge. Hence, field tests were performed to identify the influential parameters among the structural analysis options and the usage of field-measured data, and to determine the effect on the fatigue reliability assessment of the target bridge. To quantitatively compare the fatigue reliability evaluation results, field tests on an in-service steel bridge used simultaneous measurements of traffic loads and bridge responses based on the BWIM and strain gauges.

Chapter 2 describes the preparation process for evaluating the fatigue life of a target bridge. The basic information of the target bridge, category of fatigue-prone details, and field measurement are included. In addition, a frame model and a shell-solid model of the bridge were developed using commercial structural analysis programs. The effect of the accuracy of the structural analysis model on the evaluation of stress acting on the fatigue-prone detail by vehicle load was examined based on the validation results of the structural analysis model generated in two types.

Chapter 3 describes how to evaluate the fatigue life of a target bridge based on probabilistic techniques using field measurements. Two approaches for processing BWIM data were investigated. Approach 1 estimates the

equivalent truckload from the BWIM-measured gross vehicle weight (GVW) spectrum and positions the vehicle to the worst load effect in fatigue-prone details. Approach 2 generates an artificial time-series stress history by considering all BWIM-measured driving patterns, such as the entry time, driving lane, velocity, axle weights, and axle spacing of vehicles. The stress spectrum was calculated based on artificial stress history. According to each approach, fatigue reliability evaluations were performed by estimating the effective stress range (S_{eff}) and the average daily stress cycles ($ADSC$). The fatigue reliability index of each approach using BWIM data was quantitatively compared based on the fatigue reliability index evaluated using strain data.

In Chapter 4, three typical driving patterns that can be considered when performing fatigue reliability evaluation using BWIM data are investigated: headway, driving lane, and axle load distribution. Parametric studies were conducted to remove the relative influences of BWIM-measured driving patterns on fatigue reliability evaluation. The effect of each driving pattern on the fatigue life evaluation was confirmed by comparing the parametric study results with the fatigue reliability indices in Chapter 3. Consequently, parameters and evaluation procedures for reasonable fatigue life evaluation of bridges with typical short-to-medium spans were suggested.

Finally, Chapter 5 provides conclusions drawn based on the fatigue

reliability evaluation results. The importance and contributions of this study are also discussed.

CHAPTER 2

Field Tests and Analysis Models

2.1 Information of the Target Bridge

The Yong-du 1st Bridge, where the strain gauge and BWIM measurements were simultaneously performed, is a two-span steel composite bridge with a width of 25 m and length of 90 m (=2@45 m) located in Asan-si, Chungcheongnam-do, Republic of Korea. Figure 2.1 shows the target bridge.

Based on the AASHTO LRFD (AASHTO, 2020), the weld of the bottom flange and diaphragm located at the maximum moment section of box 1 of the target bridge was selected as a fatigue-prone detail. The fatigue category of the fatigue-prone detail was C'. A typical example of the base metal at the toe of a transverse stiffener-to-flange fillet weld is shown in Figure 2.2.

Figure 2.1 Yong-du 1st bridge

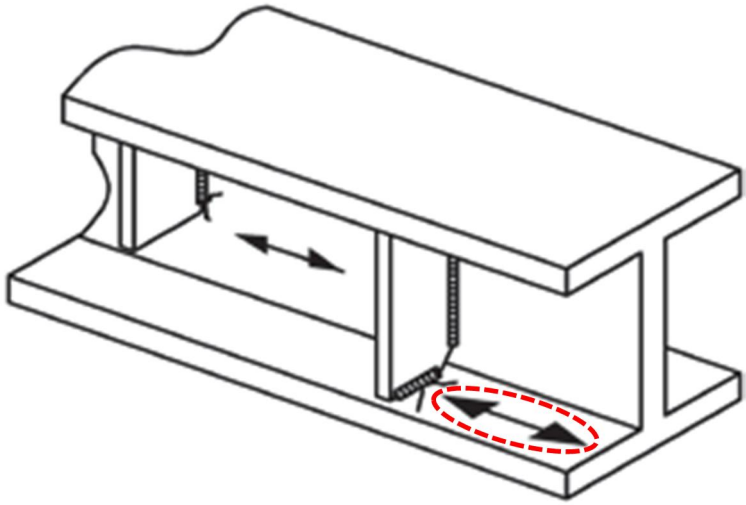

Figure 2.2 Welded stiffener-to-flange connection (AASHTO, 2020)

2.2 Field Measurement

Strain gauges were installed at one-quarter intervals on each span and 40% of the span length from both supports. The strain gauge installed on the fatigue-prone detail is 'SG-G1-4-B'. Figure 2.3 shows the installation locations of the strain gauges. The BWIM system was installed at a one-way two-lane entrance, as shown in Figure 2.4. Measurements were performed for a week from October 12th to 18th, 2019.

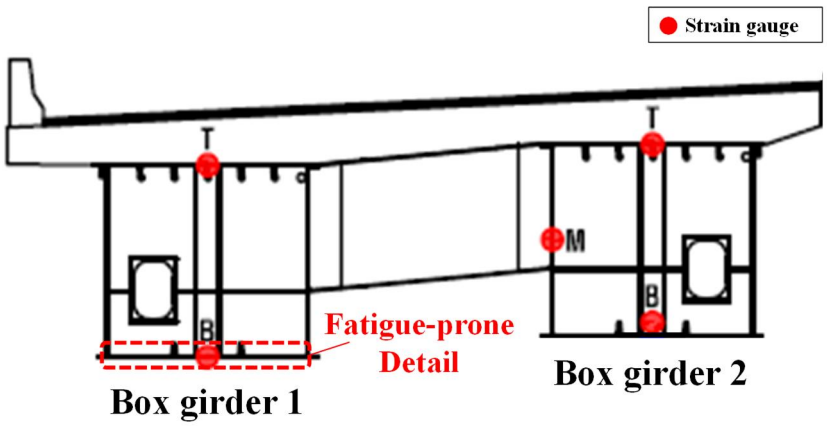

(a)

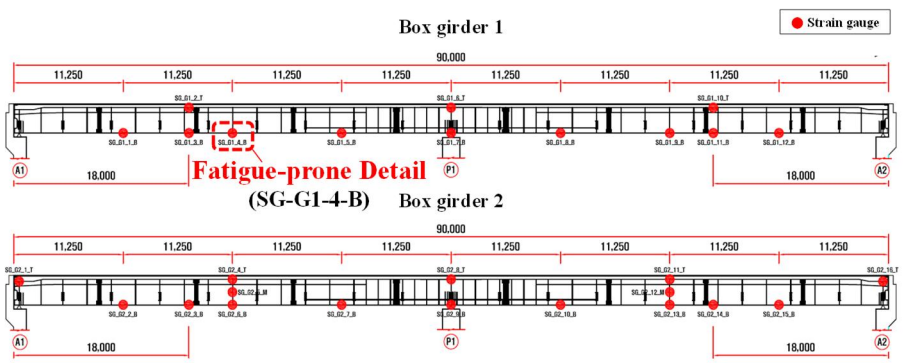

(b)

Figure 2.3 Location of the strain gauges and a fatigue-prone detail:

(a) cross-section, (b) side view

Figure 2.4 Installed BWIM system of the target bridge

2.3 Structural Analysis Model

The manual for bridge evaluation (MBE) (AASHTO, 2018) classifies structural analysis models as either simplified or refined to calculate the nominal stress acting on the fatigue-prone detail by vehicle loads. The most important difference between the two structural analysis models is whether the nominal stress applied to the fatigue-prone detail can be calculated directly. To examine the effect of the accuracy of the structural analysis model on fatigue reliability evaluation, two types of structural analysis models were developed for the target bridge using commercial structural analysis programs.

The information for each member and the material properties for the target bridge modelling are described in Appendix A.

2.3.1 Simplified Model

A three-dimensional frame model with a composite cross-section was developed using Midas civil (Midas IT, 2021). The simplified analysis model of the target bridge is shown in Figure 2.5(a), and the boundary conditions were set as shown in Figure 2.5(b) at the support node where each steel box met the pier. The frame model can be used to input the properties of the slab, web, flange, and longitudinal rib of the composite box girder section. However, there are limitations to inputting the diaphragm, horizontal stiffener, vertical stiffener, and details (i.e., fillet weld, rivet connection, and cutout).

The nominal stress applied to the fatigue-prone detail was calculated from the moment generated on the element by the vehicle load and distance from the neutral axis of the composite section to the bottom flange. Axle loads and spacing can be defined using the 'moving load function' in the program. In addition, the driving position of a vehicle was designated using the load-eccentricity function, and an influence line analysis of the nominal stress acting on the fatigue-prone detail was performed.

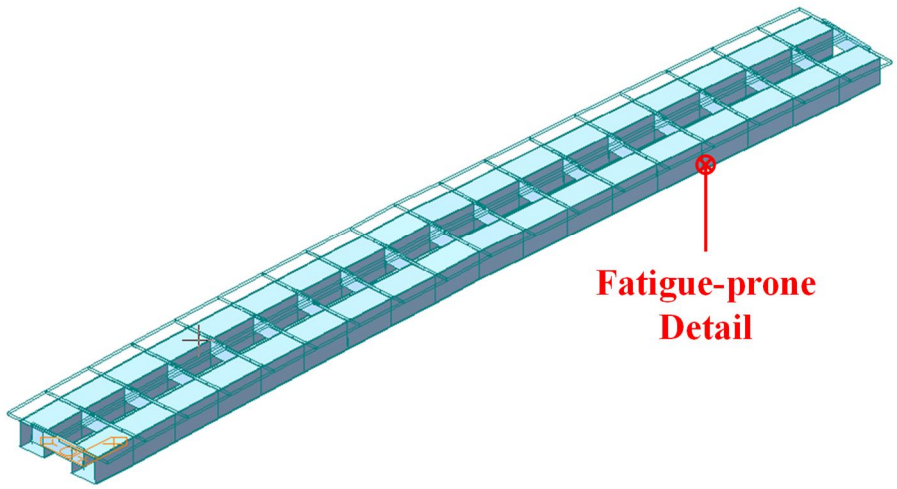

(a)

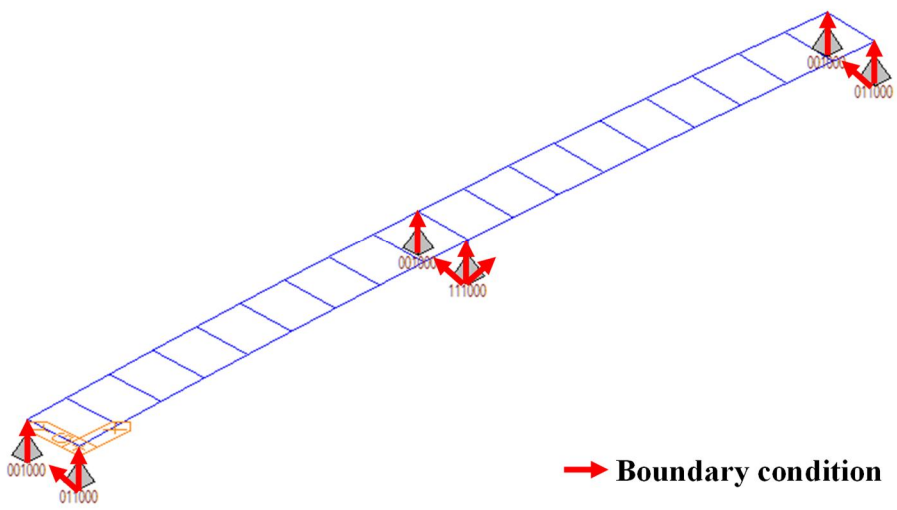

(b)

Figure 2.5 Frame model: (a) bridge model, (b) boundary conditions

2.3.2 Refined Model

A three-dimensional shell-solid model was generated using Abaqus (Dassault Systems, 2021). Two types of finite elements were used, as shown in Figure 2.6. Solid elements were used to model the bridge deck, and the steel box and crossbeam were modelled using shell elements. The solid element type is "C3D8 (8-node linear brick)," which is the most commonly used. For 'thin' shell elements with thickness less than 1/15 of the characteristic length, such as the distance between supports, the transverse shear flexibility can be neglected, and the Kirchhoff constraint must be satisfied accurately (i.e., the shell normal remains orthogonal to the shell reference surface). The shell element type is "S8R5 (8-node doubly curved thin shell, reduced integration, using 5-DOF per node)", which satisfies these conditions.

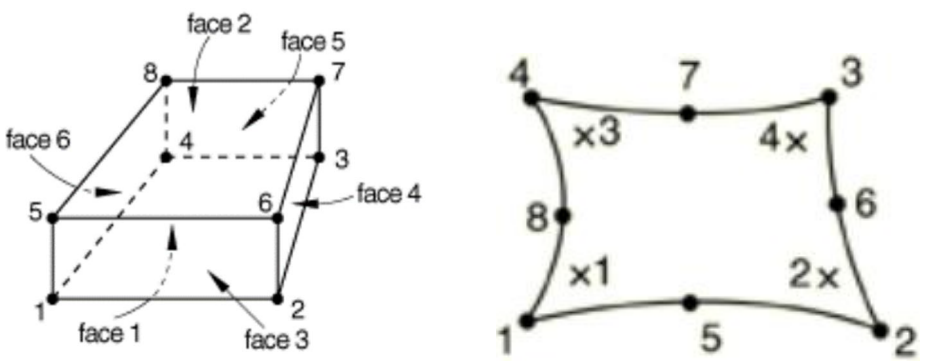

(a) **(b)**

Figure 2.6 Finite element: (a) Solid element, (b) Shell element

The refined analysis model of the target bridge is shown in Figure 2.7. Figure 2.8(a) shows the shoe placed on the support of the target bridge. To set boundary conditions similar to the real bridge, shoe elements of 500 mm × 500 mm were created and placed on the supports, as shown in Figure 2.8(b). For each DOF, the boundary conditions were set on the surface of the edges of the shoe support. The shell-solid model can implement most bridge elements and details. In this study, details related to the local stress concentration effect were not modelled because the nominal stress applied to the fatigue-prone detail is a major concern.

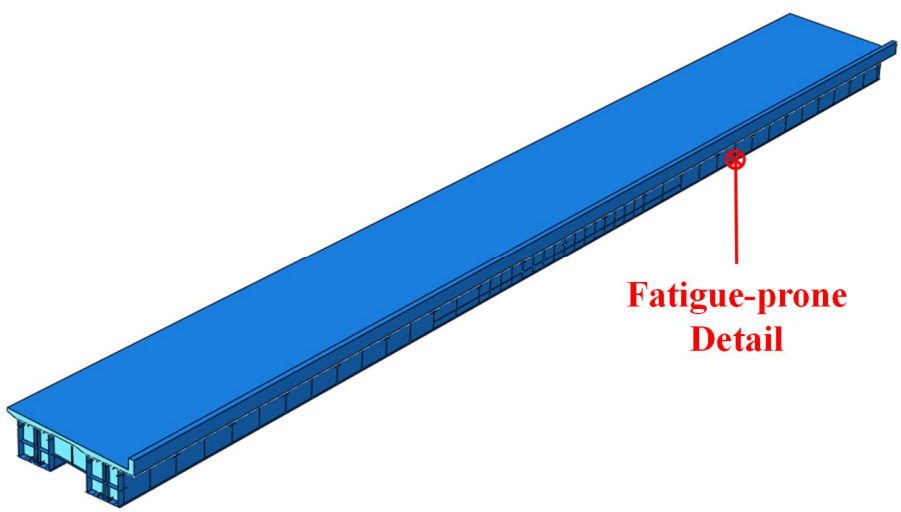

Figure 2.7 Shell-solid model

(a)

(b)

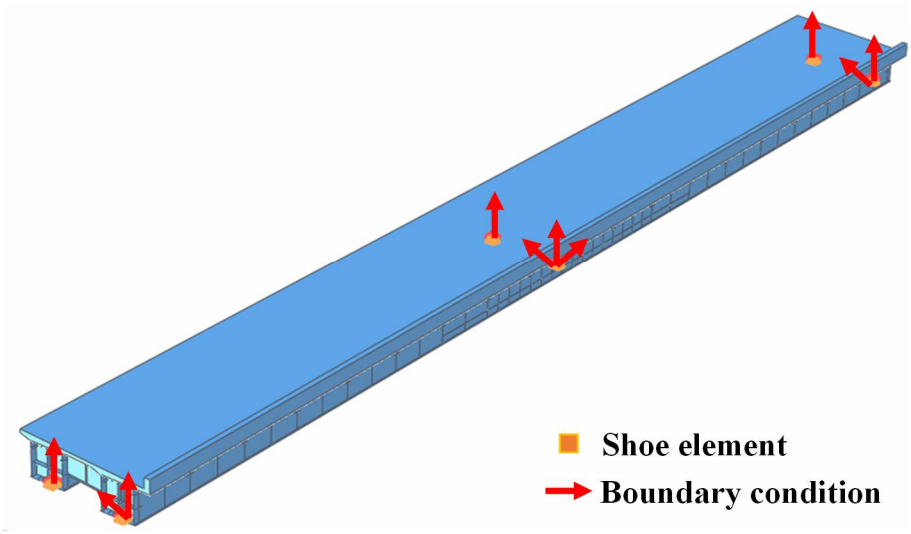

Figure 2.8 Support shoe: (a) target bridge, (b) modeling

The accuracy of the finite element analysis is affected by the mesh size of the element. Therefore, a convergence check for determining the mesh size must be preceded, which can be performed according to various criteria according to the purpose of the research. In this study, a self-weight analysis was performed to confirm the tensile stress of the maximum deflection part,

because the tensile stress occurring on the bottom flange is the most important indicator. In addition, since the two types of finite elements are combined, the convergence of the tensile stress according to the mesh size for each element was checked. The mesh size of the target element was changed to 50, 100, 150, 200, and 250 mm, while that of the other element was fixed at 200 mm. Figure 2.9 shows the convergence check results for each finite element type.

Consequently, it was confirmed that the mesh size of the solid elements constituting the concrete slab had little effect on the tensile stress of the bottom flange. In addition, the tensile stress according to the mesh size of the shell elements constituting the steel box girder was almost the same at 50 mm from 200 mm and decreased at 250 mm. Therefore, the mesh size of the shell and solid elements was determined to be 200 mm based on the convergence check results.

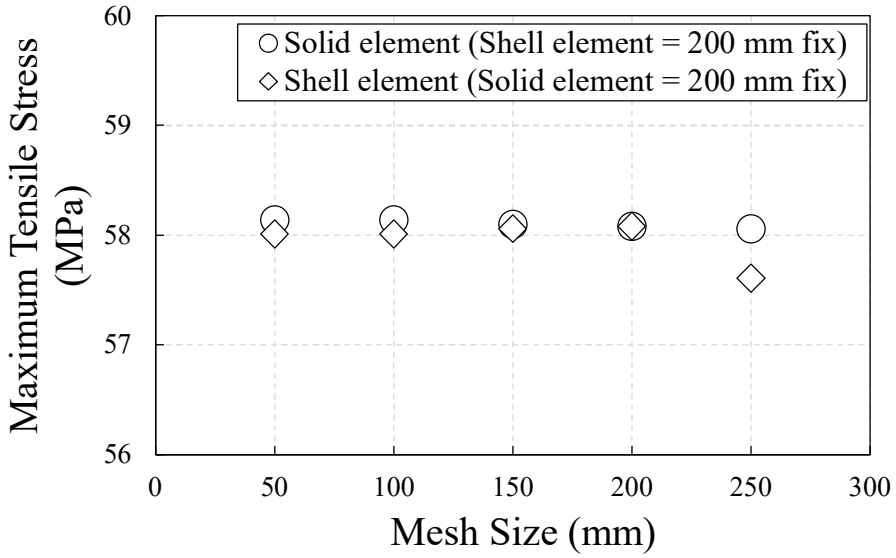

Figure 2.9 Convergence check results

To obtain the influence line of the nominal stress generated on the fatigue details, iterative static analyses were performed by moving a unit load. The unit load was applied using pressure to a rectangular wheel area of 200 mm × 600 mm, calculated based on Equation (2.1) of the Korean Highway Bridge Design Code (MOLIT, 2016).

$$A_W = \frac{12{,}500}{9} P \ \ (mm^2) \tag{2.1}$$

where, A_W is a rectangular wheel area, and P is a wheel load.

Because the nominal stress should be calculated as the membrane stress,

excluding the bending stress, the average of the upper and lower surfaces was taken. A precedent study shows that local stress concentration effects should be excluded to calculate the nominal stress of a finite element analysis model (Hobbacher, 2009). The nominal stress acting on the fatigue-prone detail was estimated by quadratic extrapolation, as shown in Figure 2.10. The reference points for extrapolation were located at 200, 400, and 600 mm along the longitudinal direction from the fatigue-prone detail.

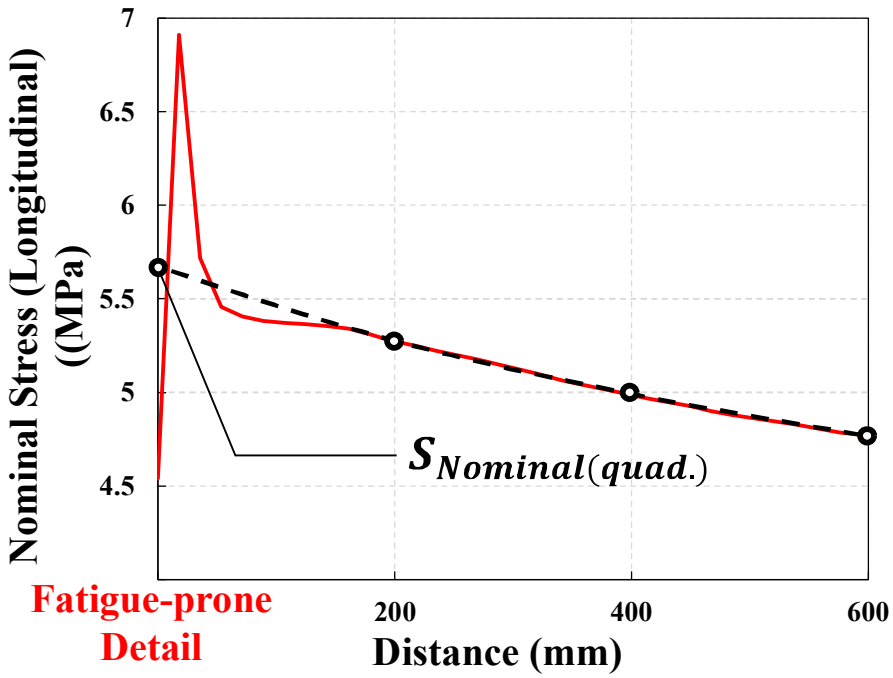

Figure 2.10 Quadratic extrapolation to determining nominal stress

2.4 Validation of Structural Analysis Model

To validate the two types of structural analysis models, cases in which a single vehicle was loaded onto the bridge were selected from the BWIM data. The measurements of the vehicle load from the BWIM data were applied to the two structural analysis models, and the difference between the calculated and measured stress ranges was obtained from the strain data.

Figure 2.11 compares the single vehicle cases. A total of 1,561 cases were identified as single vehicle loads during the entire measurement period, and the measured and calculated stress ranges are compared in Figure 2.12. Compared with the measured stress ranges from the strain data, the nominal stress ranges calculated using BWIM data averaged 12% and 4% larger in the frame model and shell-solid model, respectively. The difference between the analysis and measured results was the criterion for selecting the shell-solid model for further analysis.

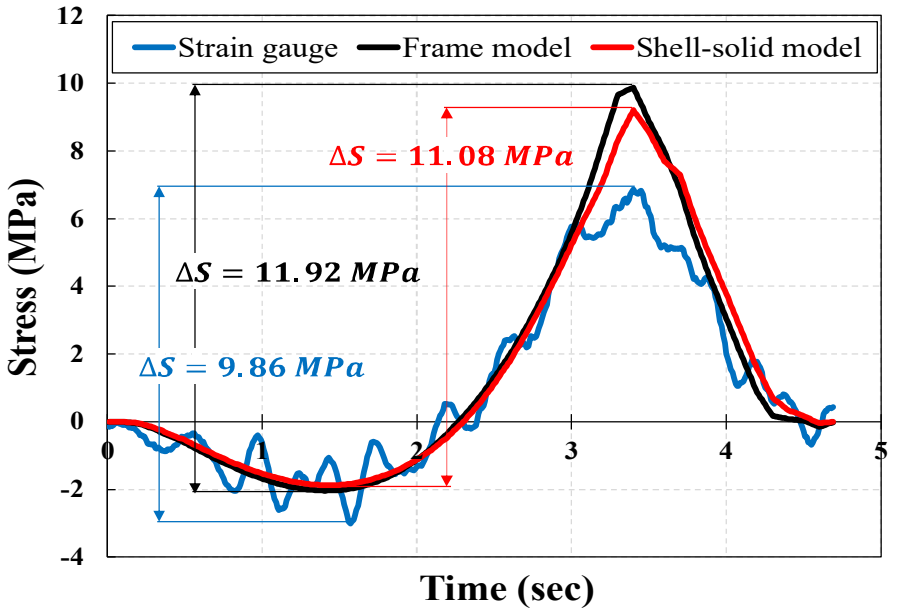

Figure 2.11 Measured and calculated stress time histories for a single vehicle loading

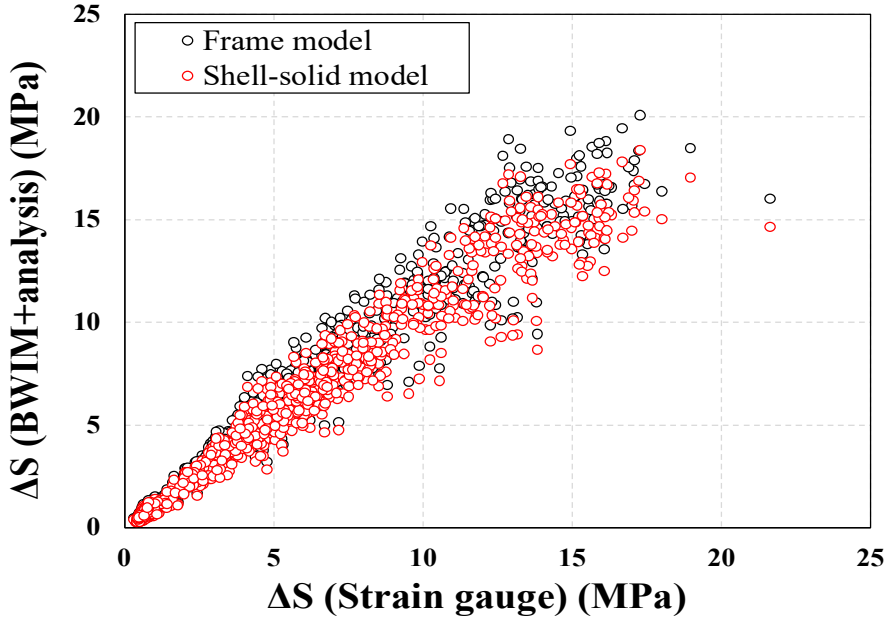

Figure 2.12 Calculated stress ranges according to two types of analysis model for all single vehicle cases

CHAPTER 3

Fatigue Reliability Evaluation

3.1 Fatigue Limit State

The limit state function of fatigue damage accumulation is defined by Equation (3.1) (Kwon and Frangopol, 2010). The fatigue damage accumulation is evaluated by the ratio of the stress cycles experienced during the service life and the limits of the stress cycles according to the fatigue category.

$$g(X) = \Delta - e \cdot D \tag{3.1}$$

where, Δ is the Miner's critical damage accumulation index in terms of resistance, e is the measurement error factor, and D is the accumulated fatigue damage defined in Equation (3.2).

$$D = \sum_i \frac{n_i(y)}{N_i} = \sum_i \frac{n_i(y) \cdot S_i}{A} \tag{3.2}$$

where, n_i is the number of cycles of the i[th] stress range (S_i) during the service life in the stress spectrum, and A is the detail-category coefficient.

The number of stress cycles applied to the fatigue-prone detail during the service life can be expressed as Equation (3.3) for the *ADSC* considering the annual traffic increase from the total stress cycles of the stress range histogram. In addition, the S_{eff} with the same number of stress cycles can be estimated as Equation (3.4) from the variable-amplitude stress range according to Miner's rule.

$$\sum_i n_i\,(\mathrm{y}) = 365 \cdot ADSC \cdot \int_0^y (1+\alpha)^y dy = 365 \cdot ADSC \cdot \frac{(1+\alpha)^y - 1}{ln(1+\alpha)} \tag{3.3}$$

where, α is the rate of annual traffic increase, and y is the number of years.

$$S_{eff} = \left[\sum_i \gamma_i\,(\Delta S_i)^3\right]^{\frac{1}{3}} \tag{3.4}$$

where γ_i is the fraction of cycles within the stress range ΔS_i.

From Equations (3.3) and (3.4), the cumulative fatigue damage in Equation (3.2) can be expressed as Equation (3.5) for the constant-amplitude S_{eff} and *ADSC*.

$$D = \sum_i \frac{n_i(y) \cdot S_i}{A} = 365 \cdot ADSC \cdot \frac{(1+\alpha)^y - 1}{ln(1+\alpha)} \cdot \frac{\left(S_{eff}\right)^m}{A} \qquad (3.5)$$

where, m is the material constant.

The parameters constituting the fatigue limit state function are described in Table 3.1.

Because most of the stress amplitudes that occur during the service life of a bridge are less than the constant-amplitude fatigue limit (CAFL), there is a risk of underestimating the fatigue damage of a bridge if the stress amplitudes at less than the CAFL are neglected. Therefore, several precedent studies have considered the stress ranges below the CAFL using a modified S-N curve based on experimental and analytical results (Kawada and Misawa, 1968; Connor et al., 2005; Yen et al., 2009; Kwon et al., 2012; Alencar et al., 2021). This study also adopted an extended S-N curve with a slope of 3 below the CAFL (Murakami et al., 2021), as shown in Figure 3.1.

The distributions of the random variables and constants for the parameters constituting the limit state function are listed in Table 1. The fatigue reliability

index (β) was estimated using the First-Order-Reliability-Method (FORM) to establish the service life.

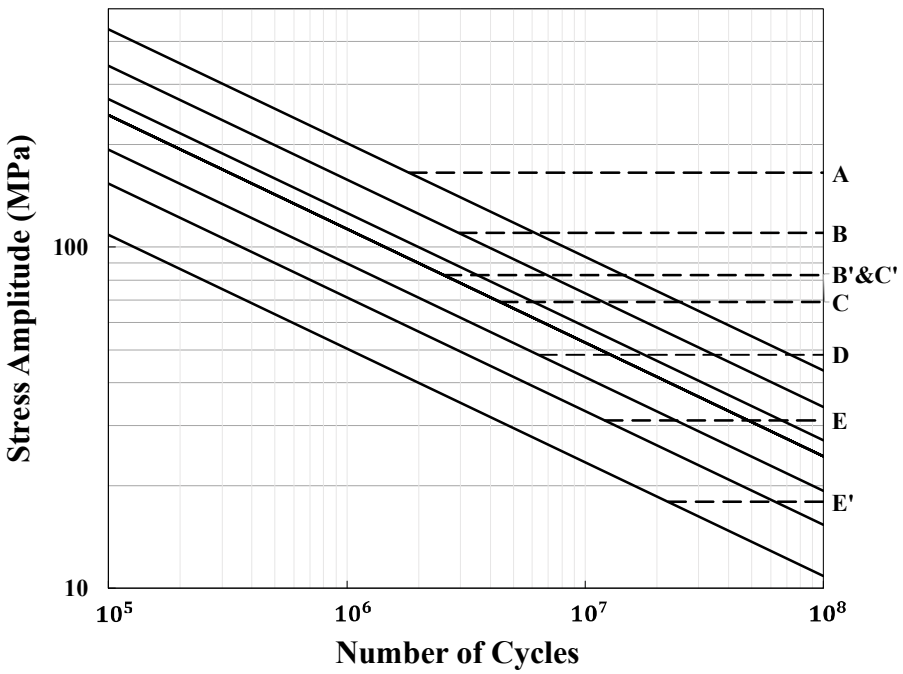

Figure 3.1 Extended S-N-curve (Murakami et al. 2021)

Table 3.1 Parameters for fatigue reliability evaluation

Parameter	Distribution		Reference
	Type	Value	
Miner's critical damage accumulation index, $\boldsymbol{\Delta}$	Lognormal	$\lambda_{\Delta} = 1, \zeta_{\Delta} = 0.3$	Wirsching, 1984
Measurement error, $\boldsymbol{e}$	Lognormal	$\lambda_{e} = 1, \zeta_{e} = 0.03$	Frangopol et al., 2008
Detail-category coefficient (MPa^3), $\boldsymbol{A}$	Lognormal	$\lambda_{A} = 23.11, \zeta_{\boldsymbol{A}} = 0.15$	Keating and Fisher, 1986; Chung, 2004
Traffic increase rate (per year), $\boldsymbol{\alpha}$	Deterministic	0.0104	Shin et al., 2007
Material constant, $\boldsymbol{m}$	Deterministic	3	AASHTO, 2020
Time (year), $\boldsymbol{y}$	variable	increment = 0.1	

3.2 Estimation of S_{eff} and *ADSC* Using Strain Data

Among the measurements for one week, only data from the five days without measurement loss or error were used for the calculation. The stress range spectrum was extracted from the field-measured stress data via the rain-flow counting method (Downing and Socie, 1982), and the *ADSC* was calculated from the results. S_{eff} was estimated according to Miner's rule.

Stress ranges lower than 7 MPa, which had little effect on fatigue damage, were excluded by applying a cutoff level (Connor et al., 2004; Hodgson et al., 2006). Because the measured period was short, the stress range spectrum was fitted as a continuous probability density function using a Gaussian mixture model (GMM). The optimal number, weights, and parameters of the GMM components were obtained iteratively using the Akaike information criterion (AIC) (Akaike, 1974). In addition, the fitted result was certified by the one-sample KS test, and the null hypothesis was not rejected at the 5% significance level. Figure 3.2 shows the stress range spectrum measured in the fatigue-prone detail and the fitting result.

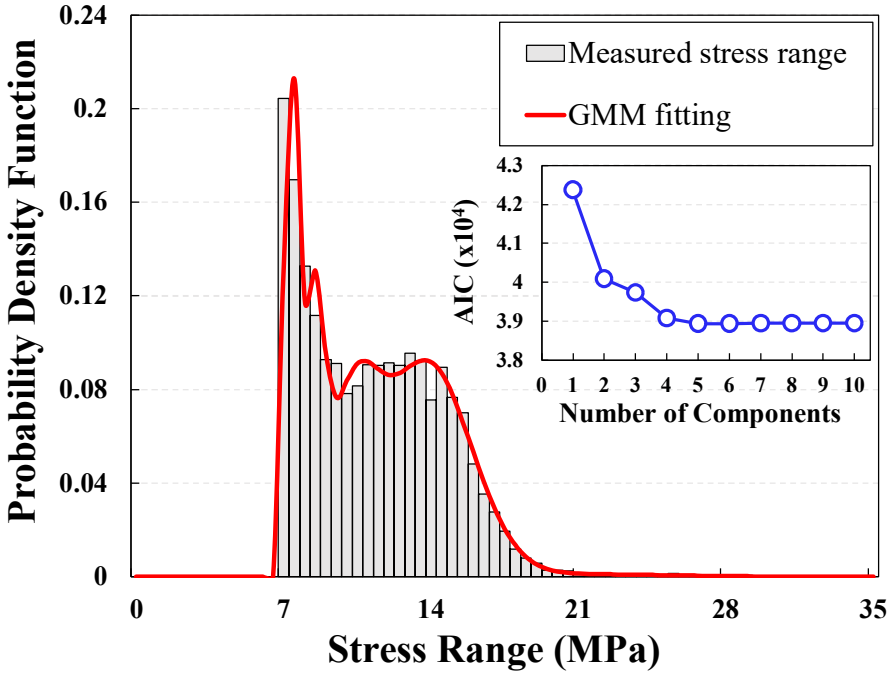

Figure 3.2 Measured stress range spectrum

3.3 Estimation of S_{eff} and *ADSC* Using BWIM Data

Prior to the estimation of S_{eff} and *ADSC*, some inaccurate measurement records of BWIM data were excluded in accordance with the precedent studies (Sivakumar et al., 2011; Kim and Song, 2019).

1) The difference between the measured GVW and the sum of the axle weights should be less than 10%.

2) GVW should be greater than 0.8 tons but less than 100 tons.

3) Vehicle length should be greater than 2 m but less than 36 m.

4) The smallest proportion of axle weight to GVW must be greater than

5%.

5) Headway should be longer than 0.3 seconds.

When fatigue evaluation is performed using BWIM data, S_{eff} and $ADSC$ can be estimated via one of the two approaches. Approach 1 is a process for estimating the equivalent truckload (W_{eq}) and single-lane average daily truck traffic ($ADTT_{SL}$) from the GVW spectrum. The GVW spectrum was fitted as a continuous probability density function using GMM. Similarly, the optimal number, weights, and parameters of the GMM components were obtained iteratively using AIC, and the fitted results were certified by the KS test. Figure 3.3 shows the GVW spectrum and the fitting results.

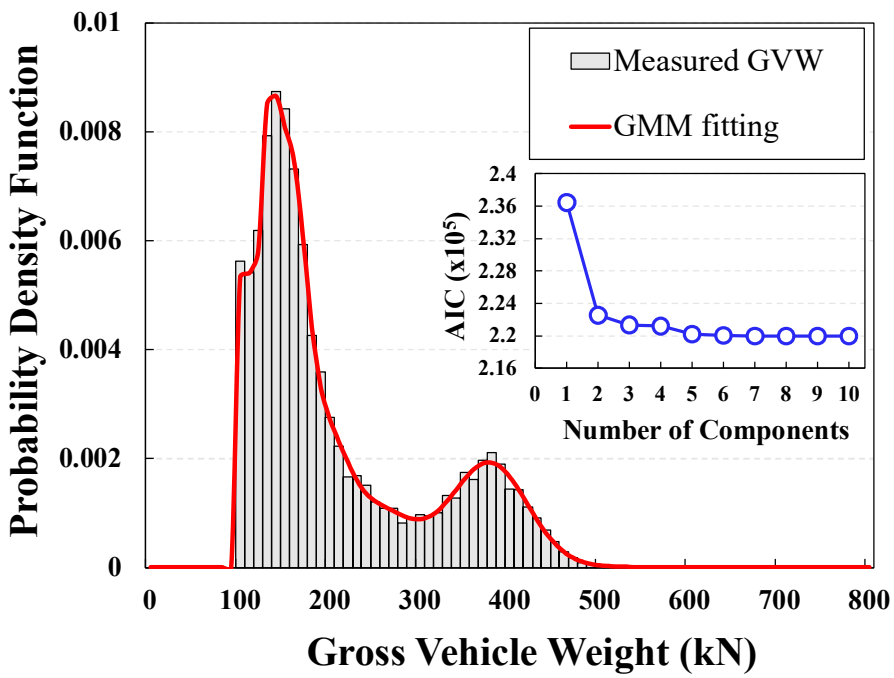

Figure 3.3 Measured GVW spectrum

W_{eq} was calculated using the root-mean-cube method shown in Equation (3.6) (Moses et al., 1987), and was applied to the location that causes the worst load effect on the fatigue-prone detail without considering traffic lanes. In this process, lightweight vehicles with contribution-to-fatigue damage of less than 100 kN were excluded from the calculation (Iatsko et al., 2020).

$$W_{eq} = \left[\sum_{i} f_i \, W_i^3\right]^{\frac{1}{3}} \tag{3.6}$$

where, f_i is the frequency of the GVW W_i.

S_{eff} can be estimated from the difference between the maximum and minimum nominal stress. To determine the vehicle location that caused the worst load effect, the influence surface of the nominal stress in the longitudinal direction was obtained, as shown in Figure 3.4(a). The influence line in Figure 3.4(b) shows the change in the nominal stress in the longitudinal direction according to the transverse position of the vehicle load at the location where the maximum nominal stress occurred. The nominal stress of the shell-solid model increased significantly as the vehicle load approached the location where the maximum stress occurred. The influence line for the longitudinal worst load effect can be extracted from the influence surface, as shown in Figure 3.4(c).

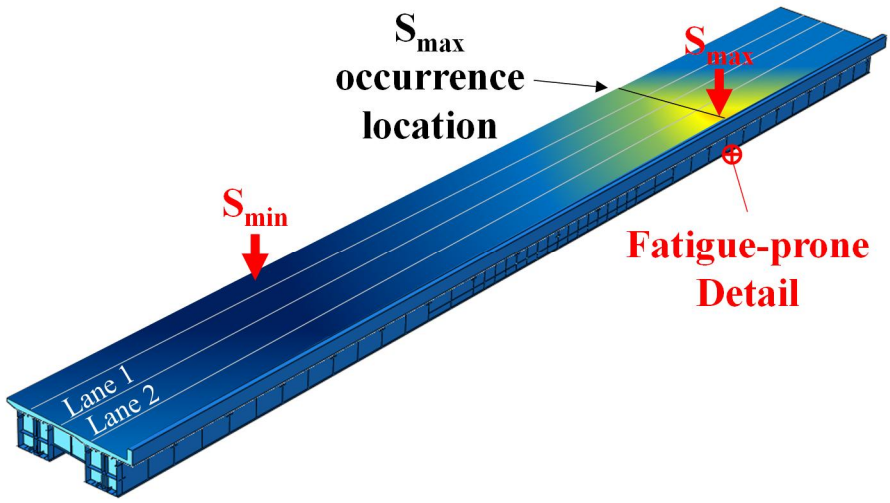
S_{max}
occurrence
location
S_{max}
S_{min}
Fatigue-prone
Detail
Lane 1
Lane 2

(a)

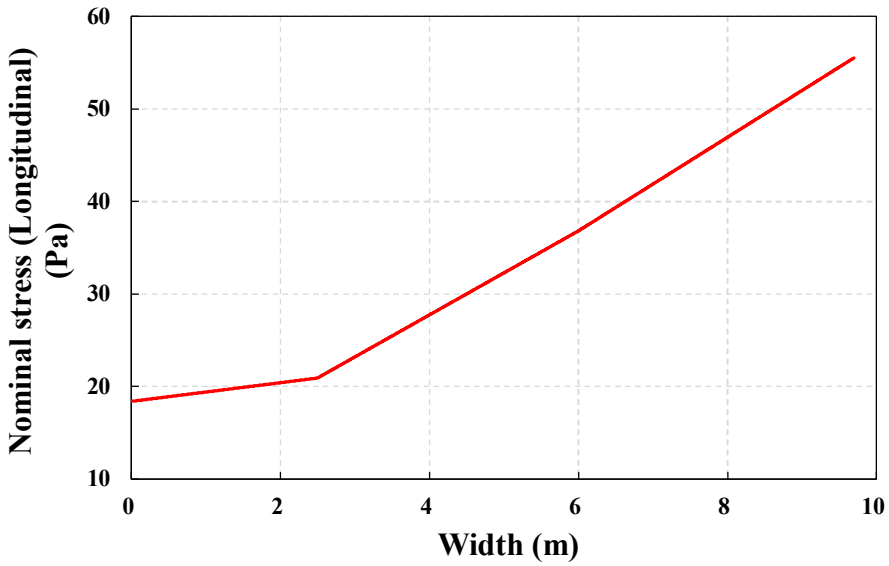
Nominal stress (Longitudinal) (Pa)
60
50
40
30
20
10
0
2
4
6
8
10
Width (m)

(b)

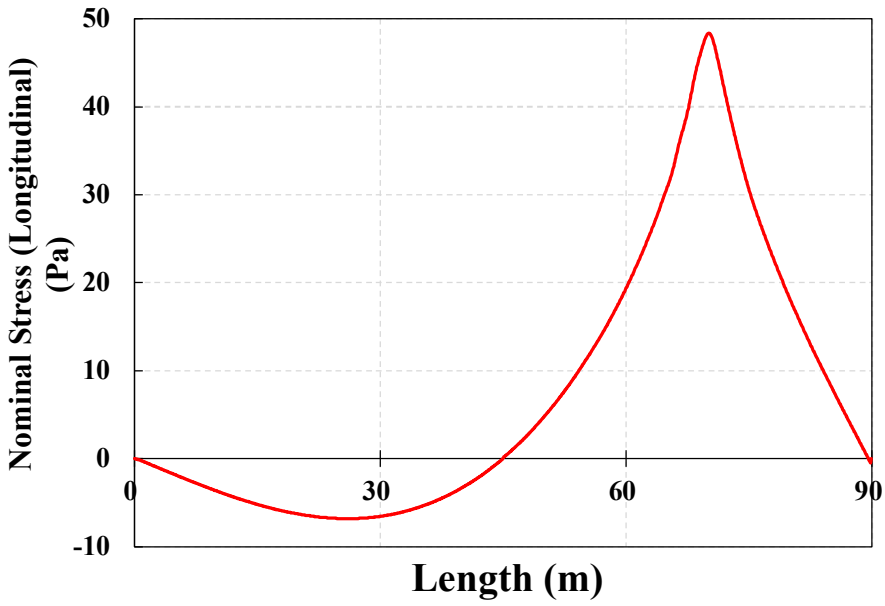

(c)

Figure 3.4. Vehicle location caused the worst load effect on fatigue-prone detail: (a) nominal stress influence surface in the longitudinal direction, (b) transversal influence line of the nominal stress at maximum stress occurrence location, (c) nominal stress influence line in the longitudinal direction

With approach 2, a time-series stress history is generated by superimposing the influence lines of multiple vehicle loads and considering all driving patterns such as entry time, driving lane, velocity, axle weights, and axle spacing of vehicles using BWIM data. Figure 3.5(a) shows the position of the vehicles along the traffic lane, and Figure 3.5(b) shows the influence lines of the nominal stress in the longitudinal direction obtained from the structural

analysis. The *ADSC* and S_{eff} were estimated using the rain-flow counting method and Miner's rule from the generated stress history. The stress spectrum was fitted as a continuous probability density function using the GMM, following the same procedure and cutoff as the strain measurement. The optimal number, weights, and parameters of the GMM components were obtained iteratively using AIC, and the fitted results were certified by the KS test. Stress ranges less than 7 MPa were excluded from the calculation. Figure 3.6 shows the stress range spectrum for the time-series stress history generated from the BWIM data and fitting results.

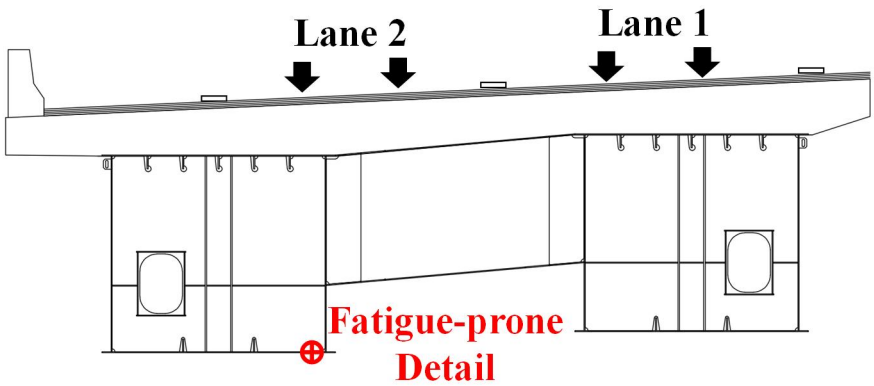

(a)

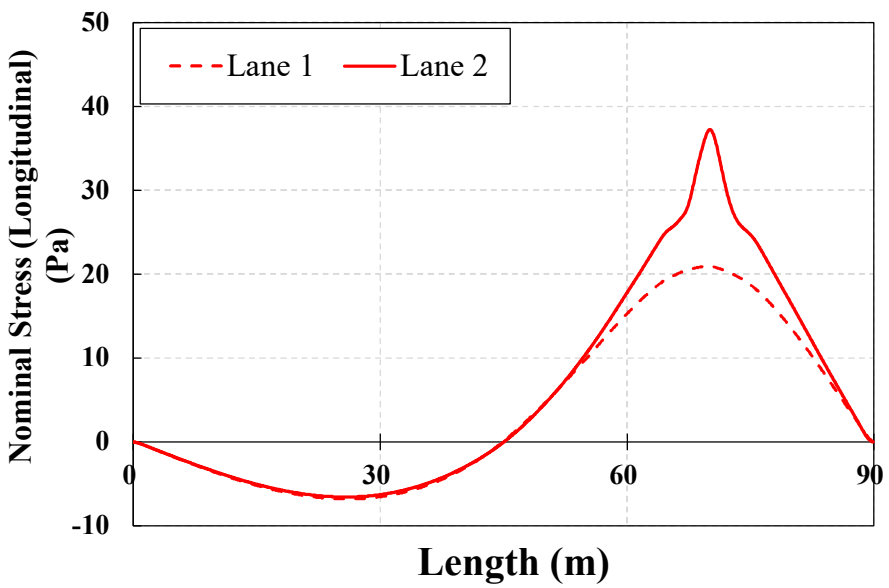

(b)

Figure 3.5 Vehicle along the traffic lane: (a) location of the vehicle, (b) nominal stress influence line at fatigue-prone detail

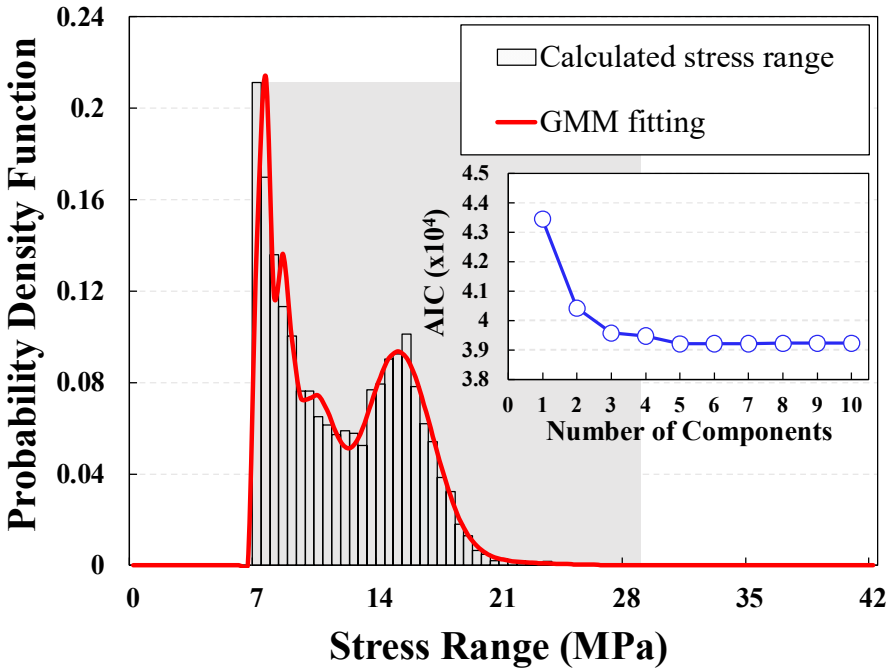

Figure 3.6 Stress range spectrum obtained from the BWIM time-series stress history

3.4 Results

Fatigue reliability analyses were performed using the strain and BWIM data. Figure 3.7 shows the results of the fatigue reliability evaluation according to the field measurement type and data-handling method. The estimated reliability index for 100 years of design life using strain measurement (β_{100yr}) was 10.42. Based on this, the fatigue life at which the fatigue reliability index of each evaluation approach equals β_{100yr} was quantitatively compared.

The fatigue life using approach 1 with BWIM data was identified as 33.8 years, and the fatigue life using approach 2 was 88.3 years. This difference in fatigue lives originates from the consideration of the driving patterns associated with the BWIM data.

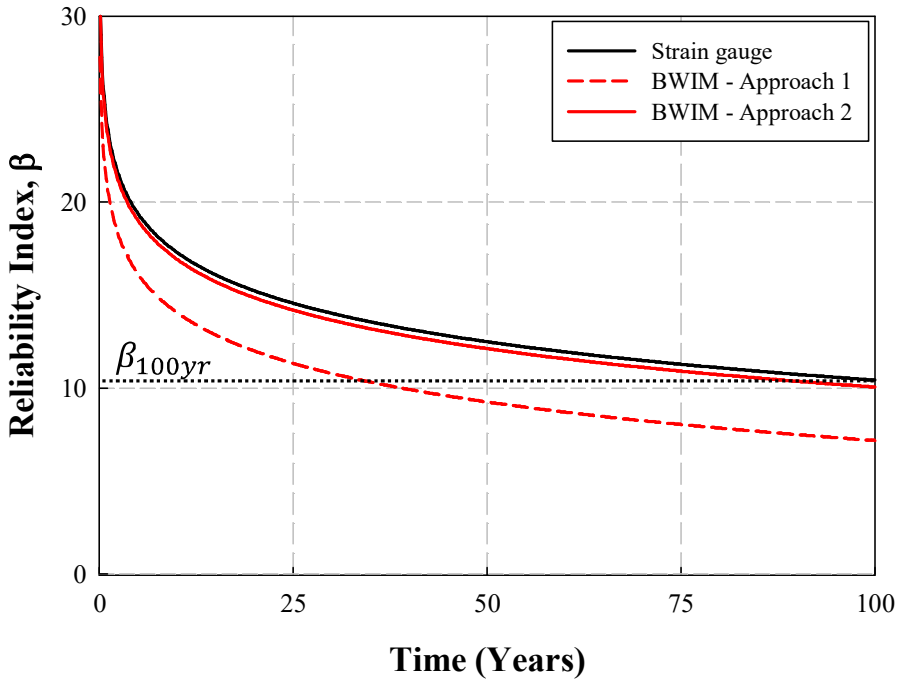

Figure 3.7 Fatigue reliability evaluation results

CHAPTER 4

Parametric Study for Driving Patterns

The driving patterns obtained from the BWIM data were identified as a critical factor in evaluating the fatigue life of the examined bridge. However, the more the driving patterns are considered, the more complex the fatigue evaluation procedure becomes. Therefore, parametric studies were conducted to identify the relative influence of each driving pattern on fatigue evaluation. The evaluation results of each case were compared with the fatigue life equal to the 100-year fatigue reliability index from the strain gauge data (β_{100yr}).

4.1 Case 1: Effect of Headway

The headway refers to the distance or time between two consecutive passing vehicles. The fatigue evaluation was based on the time-series stress history to which the headway was applied; the entry time and driving speed among the driving patterns were also considered. If the vehicles are located in the same span, the fatigue damage is evaluated to be greater owing to the superposition of vehicle loads. In other words, according to the S-N curve, the fatigue life decreased to the cube of the rate of load increase. Therefore, case 1, which additionally considered the headway in approach 1, evaluated

a larger stress range. As the stress range increased, the number of stress range cycles above the cutoff increased. Figure 4.1 shows the stress range spectrum and fitting results, and the evaluated fatigue reliability index is shown in Figure 4.2. However, in the case of the target bridge, only 8.5% of the total heavy vehicle volume was located within the same span, owing to the limited length of the bridge. It implied that with case 1, which additionally considered the headway in approach 1, the fatigue life was slightly reduced from 33.8 years to 30.1 years. This confirms that the influence of the headway is insignificant for the fatigue evaluation of bridges with a relatively short-to-medium span.

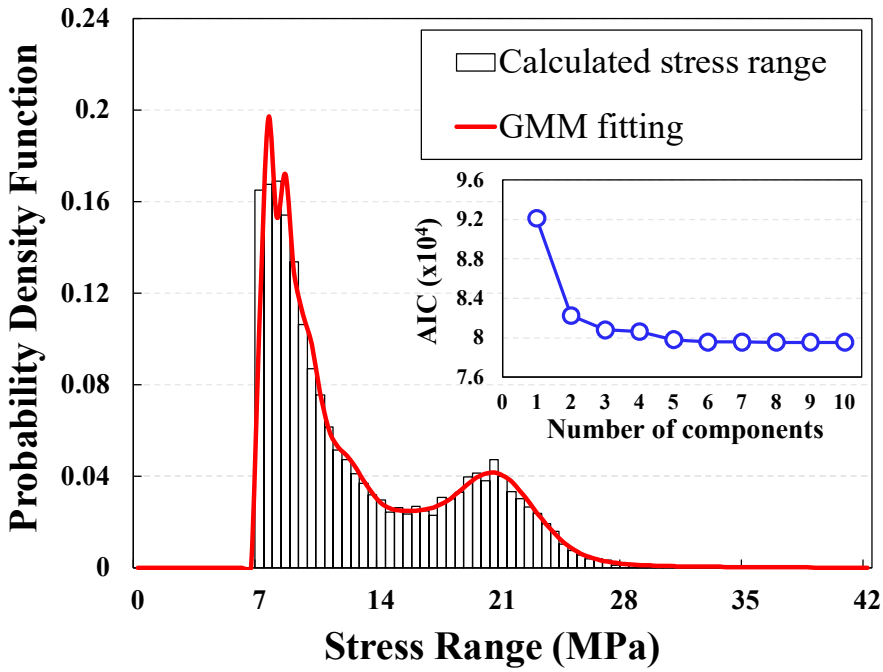

Figure 4.1 Stress range spectrum obtained from BWIM data: Case 1

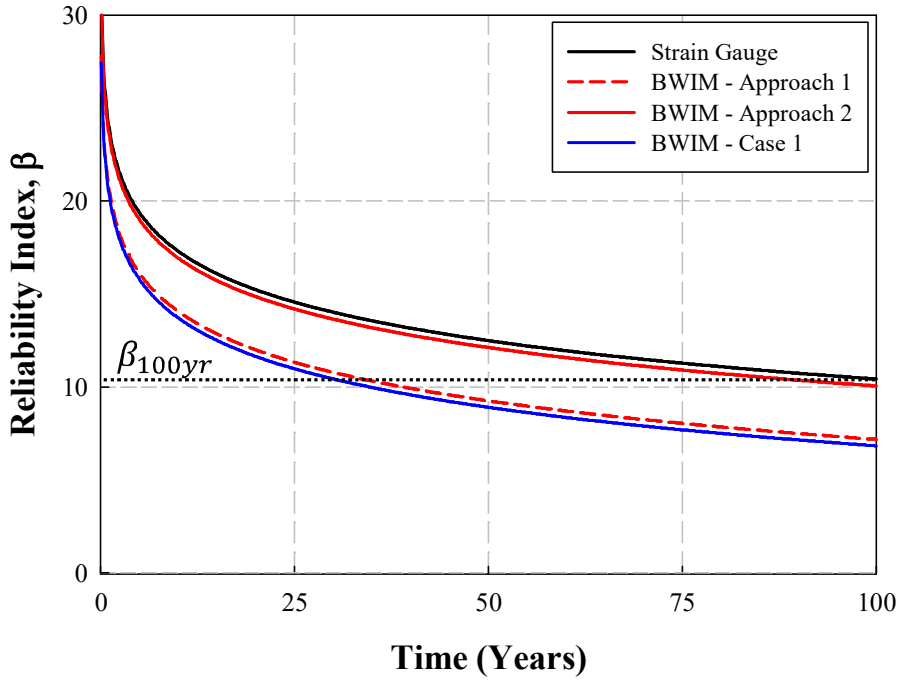

Figure 4.2 Fatigue reliability evaluation result: Case 1

4.2 Case 2: Effect of Driving Lane

Even with the same vehicle load, the stress applied to a fatigue-prone detail varies depending on the transverse position of the vehicle load, as shown in Fig. 8b. The stress range can be reduced compared to the worst load effect when the vehicles are separated into each traffic lane. As the stress range decreased, the number of stress range cycles above the cutoff decreased. Figure 4.3 shows the stress range spectrum and fitting results. The fatigue reliability index evaluated based on this is shown in Figure 4.4. The fatigue life evaluated by case 2, which additionally considers the driving lanes of

approach 1, was significantly increased from 33.8 years to 66.2 years. Therefore, the influence of driving lanes is considered a significant aspect of the fatigue evaluation of bridges.

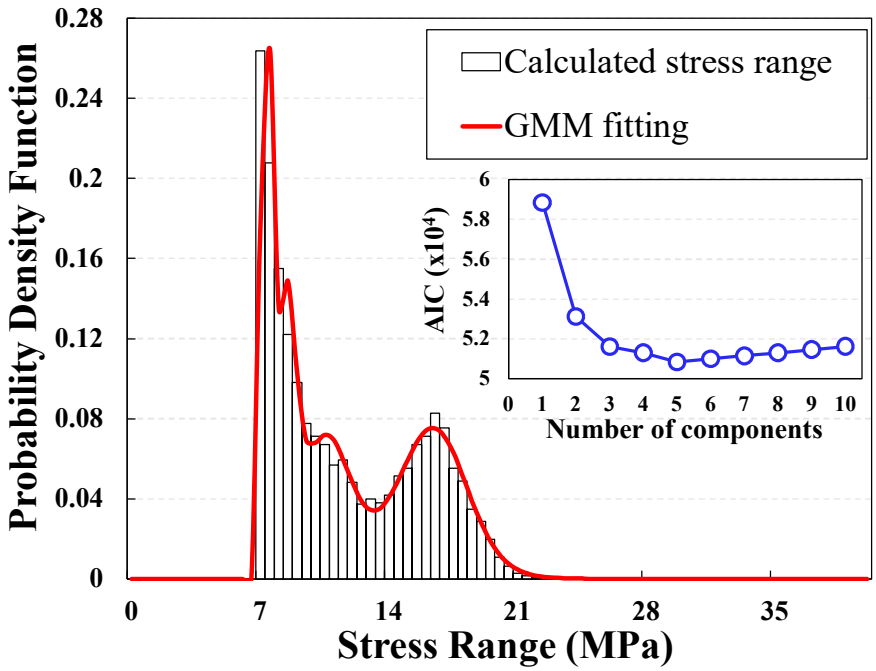

Figure 4.3 Stress range spectrum obtained from BWIM data: Case 2

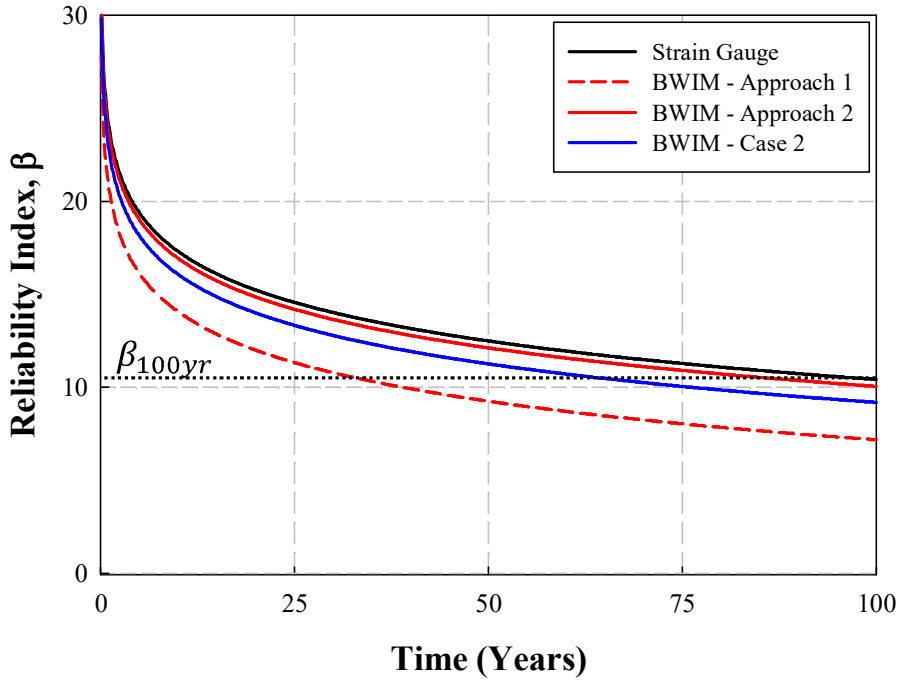

Figure 4.4 Fatigue reliability evaluation result: Case 2

4.3 Case 3: Effect of Axle Load Distribution

The axle load distribution considers vehicle weight rather than the number of wheel axles. The stress range applied to the fatigue-prone detail is reduced when the vehicle weight is considered the load distribution on the axles compared with the GVW. In addition, the influence of the axle-load distribution became more dominant for bridges with short spans. Case 3 considers the load distributed by the axles instead of the GVW used in approach 1. Figure 4.5 shows the stress range spectrum and fitting results. The fatigue reliability index evaluated based on this is shown in Figure 4.6.

The fatigue life increased from 33.8 years to 46.9 years because the stress range evaluated in case 3 was reduced. Therefore, the influence of the axle load distribution is confirmed to be essential for the fatigue evaluation of bridges with short-to-medium spans.

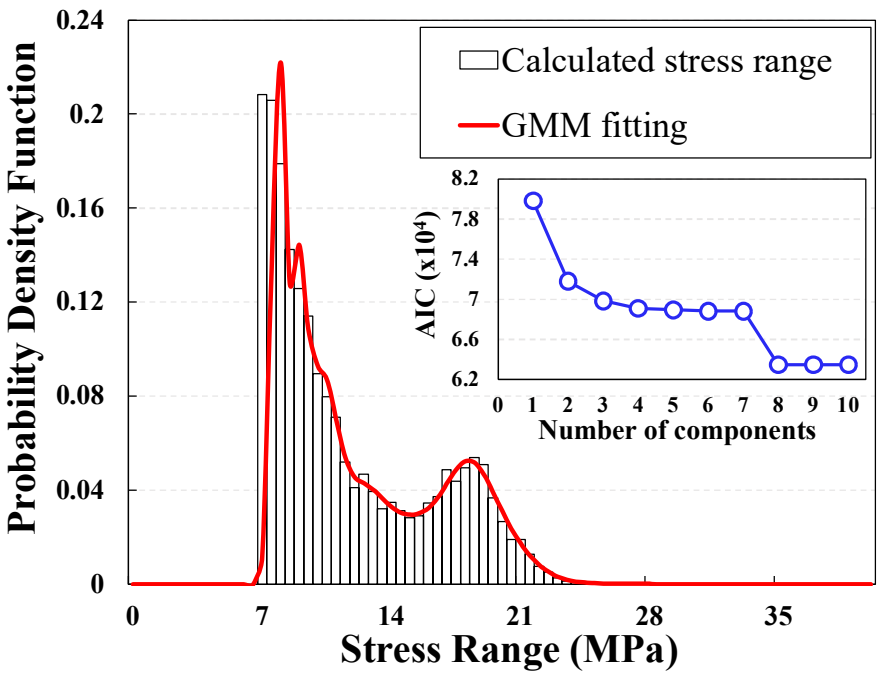

Figure 4.5 Stress range spectrum obtained from BWIM data: Case 3

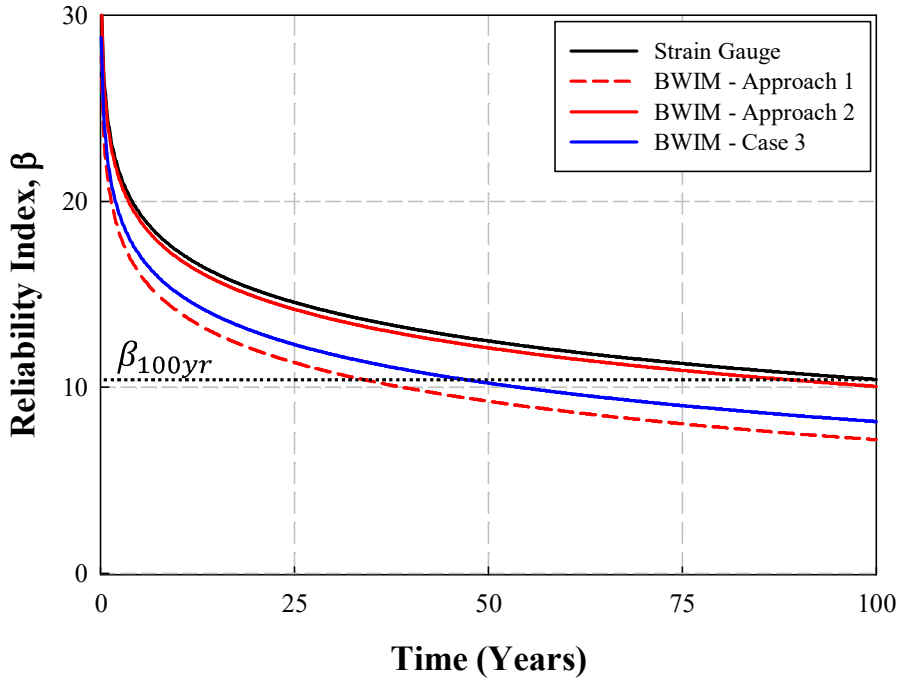

Figure 4.6 Fatigue reliability evaluation result: Case 3

4.4 Case 4: Two Driving Patterns

Based on the results of cases 1 to 3, the fatigue reliability evaluation was performed by considering the driving patterns while excluding the relatively minor influence of the headway. When calculating the stress range, the influence line for each traffic lane was used and overlapped by considering the axle weight and spacing. Because the headway of vehicles was not considered, the stress ranges applied to the fatigue-prone detail for each vehicle were encountered separately. Figure 4.7 shows the stress range spectrum and fitting results, and the fatigue reliability index evaluated based

on this is shown in Figure 4.8. In case 4, the fatigue life was significantly increased from 33.8 years to 95.8 years. Therefore, when evaluating the fatigue life of steel bridges with short-to-medium spans, approach 2 is feasible even when only the factors of the driving lane, axle weight, and axle spacing are considered.

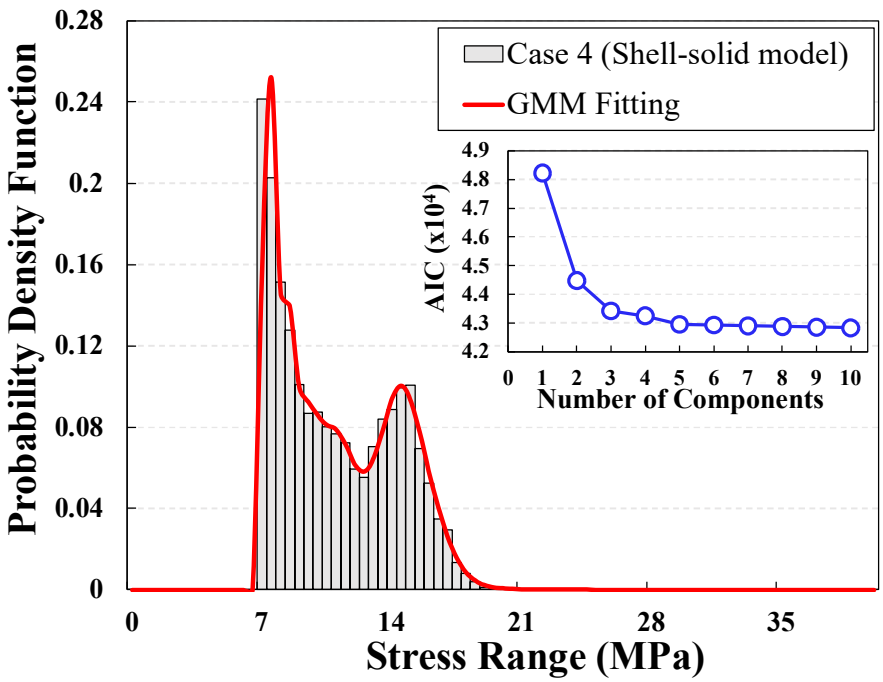

Figure 4.7 Stress range spectrum obtained from BWIM data: Case 4

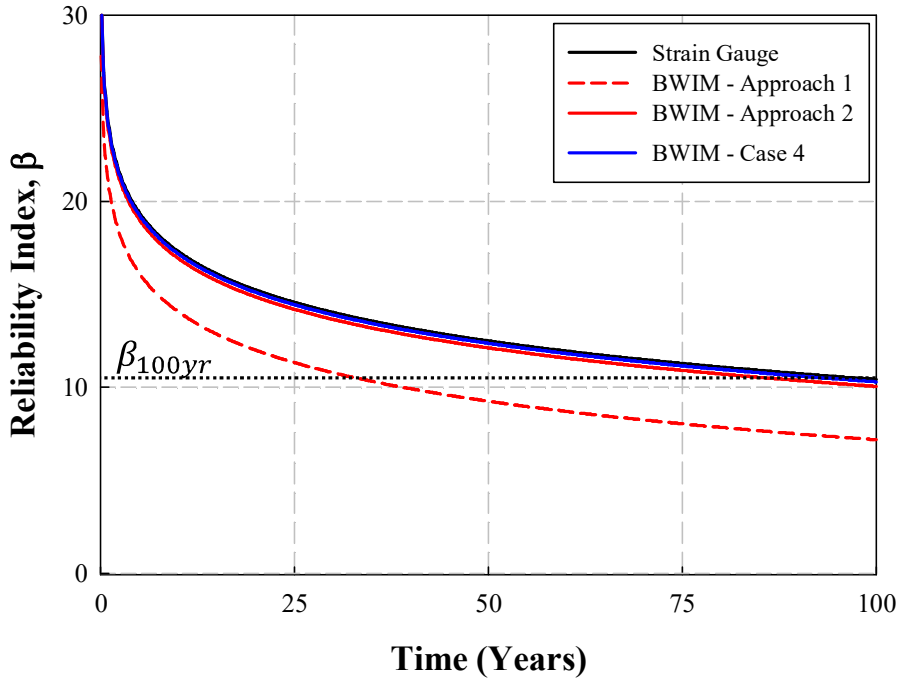

Figure 4.8 Fatigue reliability evaluation result: Case 4

4.5 Summary of Parametric Study

The considerations of the driving patterns and the results of the fatigue evaluation for each parametric study case, which includes the two approaches described in Chapter 3, are summarized in Table 4.1. The estimated fatigue reliability indices in terms of the service life are shown in Figure 4.9.

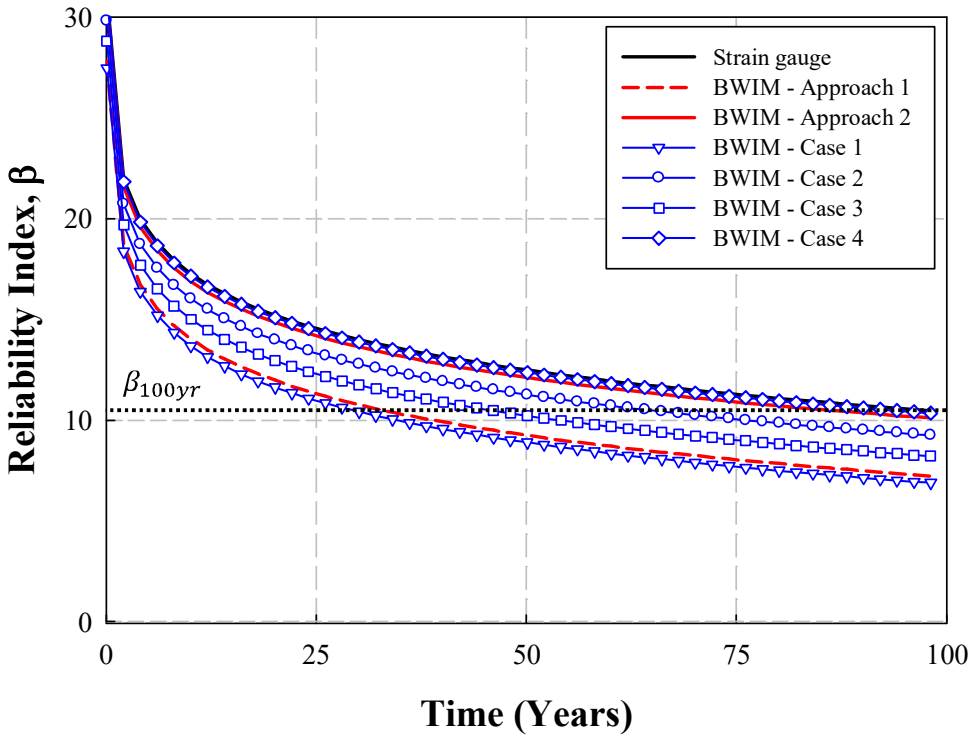

Figure 4.9 Evaluated Fatigue Reliability Indices

Table 4.1 Parametric study cases and evaluated fatigue lives

Parametric study cases	BWIM-measured driving patterns				Fatigue life (year)
	GVW	Entry time and driving speed	Driving lane	Axle weights and spacing	
Approach 1 (only GVW)	O				33.8
Approach 2 (all driving patterns)		O	O	O	88.3
Case 1 (headway)	O	O			30.1
Case 2 (driving lane)	O		O		66.2
Case 3 (axle load distribution)				O	46.9
Case 4 (two driving patterns)			O	O	95.8

CHAPTER 5

Conclusions

In this study, fatigue reliability evaluations were performed using strain gauges and BWIM data measured during the same period on an in-service steel bridge.

(1) To confirm the effect of the accuracy of the structural analysis models on fatigue evaluation using BWIM data, a frame model and a shell-solid model of the target bridge were generated using commercial structural analysis programs. The single vehicle cases were selected from the BWIM data to validate the analysis models. The same vehicle load was applied to the analysis model and compared with the strain measurement at the coincident time. As a result of comparing 1,561 cases to the stress range from strain gauge data, the nominal stress range calculated using BWIM and structural analysis models was 12% and 4% larger on average when using the frame model and the shell-solid model, respectively.

(2) The approaches that use a GVW spectrum and a time-series stress history to consider the driving patterns were investigated. Fatigue reliability evaluations were performed according to each approach

using the shell-solid model. Based on the design-life-fatigue reliability index, β_{100yr}, of strain measurement, the fatigue life in which the fatigue reliability index of each evaluation approach equaled β_{100yr} was quantitatively compared. As a result, the fatigue reliability evaluations of the fatigue life by approach 1 were three times shorter. In contrast, evaluations of fatigue life by approach 2 were 1.1 times shorter. The consideration of driving patterns using BWIM data had a significant influence on fatigue damage evaluation. Therefore, the results of this study suggest that driving patterns should be considered for the accurate fatigue life evaluation of steel bridges.

(3) For the fatigue life evaluation, parametric studies were conducted on the effect of each BWIM-measured driving pattern: entry time, driving speed, driving lane, axle weights, and spacing. In particular, the influence of the headway was relatively insignificant because vehicles were rarely located within the same span. In other words, the influences of the axle load distribution and driving lane were dominant for evaluating steel bridges with short spans. Therefore, the results of this study confirmed that it is possible to conduct an accurate strain measurement using a method similar to approach 2 and considering only the driving lane, axle weight, and axle spacing.

REFERENCE

AASHTO. (2018). *AASHTO The Manual for Bridge Evaluation.* American Association of State Highway and Transportation Officials (AASHTO). Washington, DC.

AASHTO. (2020). *AASHTO LRFD Bridge Design Specification.* American Association of State Highway and Transportation Officials (AASHTO). Washington, DC.

Akaike, H. (1974). New Look at Statistical-Model Identification. *Ieee Transactions on Automatic Control*, Ac19(6), 716-723.

Alencar, G., Hong, J.K., de Jesus, A., da Silva, J.G.S., and Calcada, R. (2021). The Master S-N curve approach for fatigue assessment of welded bridge structural details. *International Journal of Fatigue*, 152

Chotickai, P. and Bowman, M.D. (2006). Truck Models for Improved Fatigue Life Predictions of Steel Bridges. *Journal of Bridge Engineering*, 11(1), 71-80.

Chung, H.Y. (2004). *Fatigue Reliability and Optimal Inspection Strategies for Steel Bridges*. Dissertation, Civil and Environmental Engineering Department, The University of Texas at Austin, Austin, TX.

Connor, R.J., Fisher, J.W., Hodgson, I.C., and Bowman, C.A. (2004). *Results of Field Monitoring Prototype Floorbeam Connection Retrofit Details on the Birmingham Bridge.* ATLSS Report, No. 04-04, Lehigh University's Center for Advanced Technology for Large Structural Systems (ATLSS), Bethlehem, PA.

Connor, R.J., Hodgson, I.C., Mahmoud, H.N., and Bowman, C.A. (2005). *Field Testing and Fatigue Evaluation of the I-29 Neville Island Bridge over the Ohio River.* ATLSS Report, No. 05-02, Lehigh University's Center for Advanced Technology for Large Structural Systems (ATLSS), Bethlehem, PA.

Dassault Systems. (2021). *ABAQUS 2021*. Providence, RI: Dassault Systemes Simulia Corp.

Deng, Y., Li, A.Q., and Feng, D.M. (2018). Fatigue Reliability Assessment for Orthotropic Steel Decks Based on Long-Term Strain Monitoring. *Sensors*, 18(1), 181.

Deng, Y., Zhang, M., Feng, D.M., and Li, A.Q. (2021). Predicting fatigue damage of highway suspension bridge hangers using weigh-in-motion data and machine learning. *Structure and Infrastructure Engineering*, 17(2), 233-248.

Downing, S.D. and Socie, D.F. (1982). Simple Rainflow Counting Algorithms. *International Journal of Fatigue*, 4(1), 31-40.

Fisher, J.W., Kulak, G.L., and Smith, I.F.C. (1998). *A Fatigue Primer for Structural Engineers*. National Steel Bridge Alliance, U.S.A.

Fisher, J.W. and Roy, S. (2011). Fatigue of steel bridge infrastructure. *Structure and Infrastructure Engineering*, 7(8), 457-475.

Frangopol, D.M., Strauss, A., and Kim, S. (2008). Bridge reliability assessment based on monitoring. *Journal of Bridge Engineering*, 13(3), 258-270.

Guo, T., Frangopol, D.M., and Chen, Y.W. (2012). Fatigue reliability assessment of steel bridge details integrating weigh-in-motion data and probabilistic finite element analysis. *Computers & Structures*, 112245-257.

Hobbacher, A.F. (2009). The new IIW recommendations for fatigue assessment of welded joints and components - A comprehensive code recently updated. *International Journal of Fatigue*, 31(1), 50-58.

Hodgson, I.C., Connor, R.J., Mahmoud, H.N., and Bowman, C. (2006). *Approaches to the Fort Duquesne Bridge Retrofit of Fatigue and Fracture Details.* ATLSS Report, No. 06-06, Lehigh University's Center for Advanced Technology for Large Structural Systems (ATLSS), Bethlehem, PA.

Iatsko, O., Babu, A.R., Stallings, J.M., and Nowak, A.S. (2020). Weigh-in-Motion-Based Fatigue Damage Assessment. *Transportation Research Record*, 2674(8), 710-719.

Kawada, Y. and Misawa, H. (1968). The effect of stress amplitudes below endurance limit on the cumulative fatigue life. *Journal of Society of Materials Science of Japan*, 17(173), 123-127.

Keating, P.B. and Fisher, J.W. (1986). *Evaluation of FatigueTests and Design Criteria on Welded Details.* NCHRP Report, No. 286, Transportation Research Board, Washington, DC.

Kim, J. and Song, J. (2019). A Comprehensive Probabilistic Model of Traffic Loads based on Weigh-in-Motion Data for Applications to Bridge Structures. *Ksce Journal of Civil Engineering*, 23(8), 3628-3643.

Kwon, K. and Frangopol, D.M. (2010). Bridge fatigue reliability assessment using probability density functions of equivalent stress range based on field monitoring data. *International Journal of Fatigue*, 32(8), 1221-1232.

Kwon, K., Frangopol, D.M., and Soliman, M. (2012). Probabilistic Fatigue Life Estimation of Steel Bridges by Using a Bilinear S-N Approach. *Journal of Bridge Engineering*, 17(1), 58-70.

Liu, Y., Xiao, X.H., Lu, N.W., and Deng, Y. (2016). Fatigue Reliability Assessment of Orthotropic Bridge Decks under Stochastic Truck Loading. *Shock and Vibration*, 2016

Lu, N.W., Liu, Y., and Deng, Y. (2019). Fatigue Reliability Evaluation of Orthotropic Steel Bridge Decks Based on Site-Specific Weigh-in-Motion Measurements. *International Journal of Steel Structures*, 19(1), 181-192.

Lu, N.W., Noori, M., and Liu, Y. (2017). Fatigue Reliability Assessment of Welded Steel Bridge Decks under Stochastic Truck Loads via Machine Learning. *Journal of Bridge Engineering*, 22(1),

Mao, J.X., Wang, H., and Li, J. (2019). Fatigue Reliability Assessment of a Long-Span Cable-Stayed Bridge Based on One-Year Monitoring Strain Data. *Journal of Bridge Engineering*, 24(1), 05018015.

Midas IT. (2021). *MIDAS Civil 2021*. Providence, RI: MIDAS Information Technology Corp.

Miner, M.A. (1945). Cumulative Damage in Fatigue. *Journal of Applied Mechanics-Transactions of the Asme*, 12(3), 159-164.

MOLIT. (2016). *Korean Highway Bridge Design Code (Limit State Design Method).* Ministry of Land, Infrastructure, and Transport (MOLIT). Sejong-si.

Moses, F., Schilling, C.G., and Raju, K.S. (1987). *Fatigue Evaluation Procesdures for Steel Bridges.* NCHRP Report, No. 299, Transportation Research Board, Washington, DC.

Murakami, Y., Takagi, T., Wada, K., and Matsunaga, H. (2021). Essential structure of S-N curve: Prediction of fatigue life and fatigue limit of defective materials and nature of scatter. *International Journal of Fatigue*, 146

Ni, Y.Q., Ye, X.W., and Ko, J.M. (2010). Monitoring-Based Fatigue Reliability Assessment of Steel Bridges: Analytical Model and Application. *Journal of Structural Engineering*, 136(12), 1563-1573.

Ni, Y.Q., Ye, X.W., and Ko, J.M. (2012). Modeling of Stress Spectrum Using Long-Term Monitoring Data and Finite Mixture Distributions. *Journal of Engineering Mechanics*, 138(2), 175-183.

Nyman, W.E. and Moses, F. (1985). Calibration of Bridge Fatigue Design-Model. *Journal of Structural Engineering-Asce*, 111(6), 1251-1266.

Shin, D.K., Kwon, T.H., and Park, Y.S. (2007). Reliability Analysis of Fatigue Truck Model Using Measured Truck Traffic Statistics. *Journal of Korean Society of Steel Construction*, 19(2), 211-221.

Sivakumar, B., Ghosn, M., and Moses, F. (2011). *Protocols for Collecting and Using Traffic Data in Bridge Design.* NCHRP Report, No. 683, Transportation Research Board, Washington, DC.

Wirsching, P.H. (1984). Fatigue Reliability for Offshore Structures. *Journal of Structural Engineering*, 110(10), 2340-2356.

Yan, D.H., Luo, Y., Lu, N.W., Yuan, M., and Beer, M. (2017). Fatigue Stress Spectra and Reliability Evaluation of Short- to Medium-Span Bridges under Stochastic and Dynamic Traffic Loads. *Journal of Bridge Engineering*, 22(12),

Yan, D.H., Luo, Y., Yuan, M., and Lu, N.W. (2017). Lifetime fatigue reliability evaluation of short to medium span bridges under site-specific stochastic truck loading. *Advances in Mechanical Engineering*, 9(3),

Yen, B.T., Hodgson, I.C., Zhou, E., and Crudele, B.B. (2009). *Estimation of Fatigue Life below CAFL* 2nd International Conference on Fatigue and Fracture in the Infrastructure, Bethlehem, PA.

APPENDIX

A. Information of Bridge Members

A.1 Steel box girder

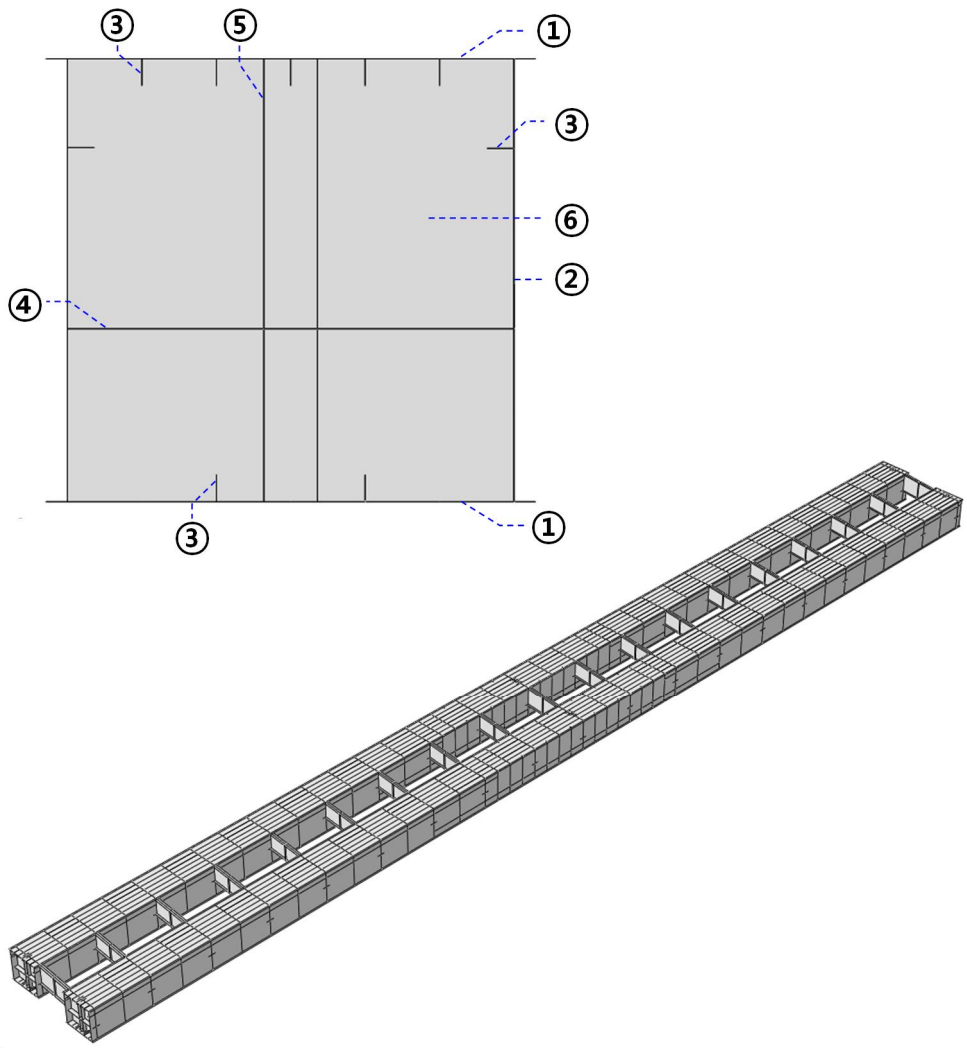

Figure A. 1 Steel box girder

Table A. 1 Information of steel box girder member

Bridge element		t (mm)	Steel grade
① Top/bottom flange		14	SM490A*
② Web		12	SM490A*
③ Top/bottom longitudinal rib		12	SM400A**
④ Horizontal stiffner		12	SM400A**
⑤ Vertical stiffener	Support	20	SM490A*
	Else	12	SM400A**
⑥ Diaphragm	Middle support	20	SM490A*
	End support	12	SM490A*
	Else	12	SM400A**

* SM490A: $F_{u.min}$ = 490MPa

** SM400A: $F_{u.min}$ = 400MPa

A.2 Crossbeam

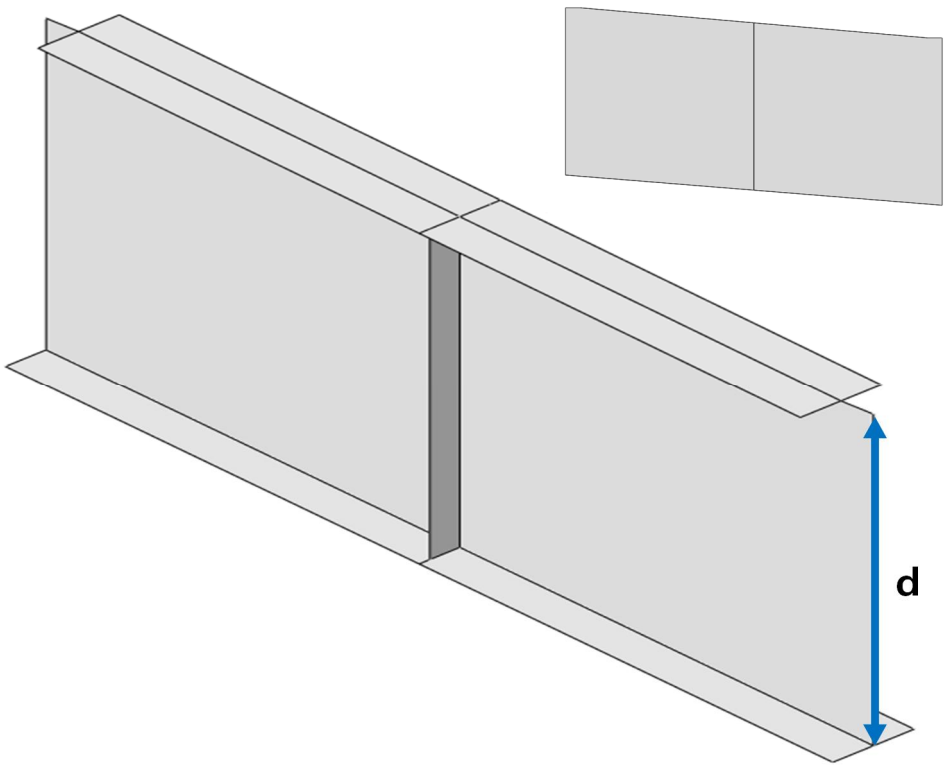

Figure A. 2 Crossbeam

Table A. 2 Information of cross beam member

Bridge element		d (mm)	t (mm)	Steel grade
Crossbeam	Support	1500	12	SM490A*
	Else	1250	12	SM400A**

* SM490A: $F_{u.min}$ = 490MPa

** SM400A: $F_{u.min}$ = 400MPa

A.3 Concrete slab

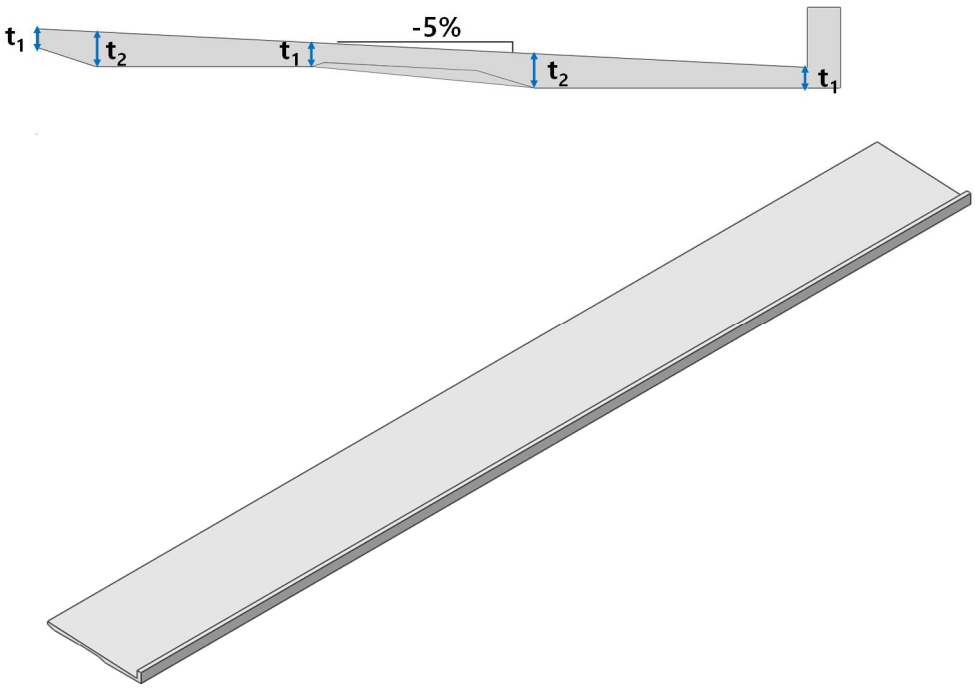

Figure A. 3 Concrete slab

Table A. 3 Information of concrete slab

Bridge element	t_1 (mm)	t_2 (mm)	Mass density (ton/m^3)	Young's modulus (MPa)	Poisson's ratio
Concrete slab	240	750	2500	24500	0.167

국 문 초 록

이상현
건설환경공학부
서울대학교 대학원

이 연구에서는 현장계측된 변형률 및 BWIM 데이터를 활용한 공용 중 강 교량의 피로수명을 확률론적으로 평가하는 전반적인 절차 및 방법에 대해 검토하였다.

현장계측의 종류에 따른 피로 신뢰도 평가 결과의 차이를 정량적으로 검토하기 위해 실제 공용 중인 강 교량에서 동일한 기간동안 변형률 및 BWIM 계측을 수행하였다. 또한, BWIM 데이터를 활용한 피로 평가 시 활용되는 구조해석모델의 정밀성이 평가 결과에 미치는 영향에 대해 확인하기 위해, 뼈대구조요소 단순해석모델과 유한요소 상세해석모델을 각각 상용 구조해석 프로그램을 이용하여 구축하였다.

선행연구 조사 결과들을 바탕으로, BWIM 데이터와 구조해석모델을 활용하여 교량 부재의 피로 취약 상세에 가해지는 유효응력범위 및 반복응력횟수를 추정하는 두 가지 처리 기법을 정의하였다. 일반적으로 가장 정확한 평가 방법으로 인식되는 변형률 계측 데이터를 활용한 방법을 기준으로, 두 BWIM 데이터 처리 기법에 따른 피로 신뢰도 평가 결과를 비교하였다. 비교된 피로 신뢰도 평가 결과를 통해 BWIM 데이터 처리 시 고려되는 주행 패턴들이 평가 피로 수명에 큰 영향을 미침을 확인하였다.

마지막으로, BWIM 데이터로부터 고려될 수 있는 대표적인 3가지 주행 패턴(연행 효과, 주행 차선, 축 하중 분산)을 정의하고, 각 주행 패턴이 평가 결과에 미치는 영향에 대한 검토를 수행하였다. 평가 대상 교량과 같은 일반적인 단-중 경간의 강

교량의 경우, 차량 하중의 연행에 의한 동시 재하보다는 차량의 주행 차선 및 차축에 의한 하중 분산 효과가 교량의 피로 수명을 평가하는데 있어 보다 지배적인 영향을 미치며, 이 두 가지 주행 패턴만을 고려하더라도 변형률 데이터에 의한 평가 결과만큼 충분히 정확한 피로 수명의 평가가 가능함을 확인하였다.

주요어: 강 교량, 피로, 신뢰도 평가, 현장 계측, 변형률, Bridge weigh-in-motion (BWIM), 유한요소모델

학번: 2020-22553